Christina Mauerhofer, BSc.

View of the pre-60S maturation in a temporal manner

MASTER'S THESIS

to achieve the university degree of

Master of Science

Master's degree programme: Molecular Microbiology

submitted to

Graz University of Technology

Supervisor

Ao. Univ.-Prof. Dr. Helmut Bergler

Institute of Molecular Biosciences

Co-Supervisor
Heimo Wolinski, PhD.

Graz, February 2015

AFFIDAVIT

I declare that I have authored this thesis independently, that I have not used other than the declared sources/resources, and that I have explicitly indicated all material which has been quoted either literally or by content from the sources used. The text document uploaded to TUGRAZonline is identical to the present master‘s thesis dissertation.

Date

Signature

Mein besonderer Dank gilt:

Helmut, für die engagierte und hilfreiche Betreuung. Es hat mich sehr gefreut einen so leidenschaftlichen Wissenschaftler kennengelernt haben zu dürfen, der stets eine Antwort parat hat!

Der gesamten Bergler-Crew, allen voran Gertrude und Mathias für die zahlreichen Ratschläge und auch so manch schönen Stunden.

Heimo Wolinski und Klara Hellauer für die tatkräftige Unterstützung bei der Mikroskopie sowieso sehr guten Ratschlägen für die anschließende Bildbearbeitung. Und natürlich auch für ein offenes Ohr, wenn es einmal nicht so gut klappte.

Meiner Familie, die mich unterstützt, immer an mich glaubt, immer zu mir hält und ohne die ich diese Arbeit nicht schreiben könnte.

Meinem Freund Peter für die liebevolle Begleitung während meiner Studienzeit. Du bist immer meine starke Schulter, an die ich mich anlehnen kann.

Meinen Freunden, die mich schon sehr lange begleiten und mir viel Spaß und Freude abseits des Laboralltags bereiten.

Zusammenfassung

Ribosomen sind komplexe Fabriken zur Erzeugung zellulärer Proteine, weshalb ihre Biogenese einen essentiellen, konservierten Prozess darstellt, der in *Saccharomyces cerevisiae* ausführlich untersucht wurde. Ribosomen bestehen aus einer kleinen (40S) und einer großen (60S) Untereinheit und an ihrer Biogenese sind mehr als 200 nicht ribosomale Faktoren, 75 snoRNAs und alle drei RNA Polymerasen beteiligt. Die Ribosomenbiogenese startet mit der Transkription einer 35S pre-rRNA im Nukleus, welche anschließend modifiziert und prozessiert wird. Währenddessen assemblieren ribosomale und nicht ribosomale Proteine und formen dabei das erste pre-ribosomale Partikel, das ununterbrochen durch dynamisches, kaskadenartiges Anlagern und Ablösen immer weiterer Faktoren verändert und währenddessen ins Nukleoplasma und weiter ins Zytoplasma geschleust wird. Ein entscheidender Schritt ist dabei die Assemblierung von Drg1, das den Angriffspunkt von Diazaborin darstellt, an frisch exportierte pre-60S Partikel. Diese AAA-ATPase katalysiert die Ablösung des Shuttling Proteins L24, eine Reaktion, die die Voraussetzung für alle nachfolgenden zytoplasmatischen Reifungsschritte darstellt.

Die Struktur und Assemblierung von Ribosomen ist bis auf ihre zeitliche Abfolge derzeit gut charakterisiert. Deshalb bestand das Ziel dieser Arbeit in der zeitlichen Charakterisierung der Ribosomenbiogenese unter Diazaborin Einfluss zusätzlich zur Untersuchung des Einflusses von Diazaborin auf frühe Schritte der Ribosomenbiogenese. Weil die Depletion von Rpl40 zu ähnlichen Effekten wie die Inaktivierung von Drg1 führen sollte, wurden zusätzlich die Einflüsse von Rpl40 auf zytoplasmatische Reifungsschritte mittels TAP- Reinigung und Immunfluoreszenz untersucht.

Bei der zeitlichen Analyse des Shuttling-Faktors Bud20 wurden ohne Behandlung 90% des Proteins im Kern detektiert und verringerten sich auf 29% nach 5 Minuten Diazaborin Behandlung. Von Nog1 befanden sich ohne Behandlung 83% im Kern, im Gegensatz zu 29% nach 30 Minuten Diazaborin Behandlung. Bei der Analyse der nukleolären Lokalisierung von Nog1 wurden 25% des Signals ohne Behandlung und 6% nach 10 Minuten Diazaborin Behandlung im Kern detektiert. Die Untersuchung des nukleolären Faktors Nop58 zeigte dessen Akkumulierung in subnukleoplasmatischen Punkten. Der nukleoläre Faktor Noc2 verhielt sich im Gegensatz zu dem spät nukeolären Faktor Nsa1 ähnlich wie Nop58. Der Reifungsfaktor Noc2 wies zusätzlich eine hohe Colokalisierung mit der RNA Polymerase I nach Diazaborin Behandlung auf. Die weitere Analyse von Nop58-TAP Partikeln zeigte grundsätzlich keine starken Veränderungen in der Partikelzusammensetzung. Diese Resultate führten zu der Hypothese, dass es unterschiedliche Kontrollsysteme für unterschiedlich weit fortgeschrittene Partikel gibt.

Abstract

Ribosomes are the molecular machines translating the genetic code into proteins and consist of large (60S) and small (40S) subunits formed from 5 rRNAs and ribosomal proteins. Their biogenesis is a very complex and energy consuming pathway involving 200 trans acting factors, 76 snoRNAs and all three RNA polymerases. Since this process is highly conserved across eukaryotes, ribosome biogenesis is well investigated in the model organism *Saccharomyces cerevisiae*. The biogenesis starts in the nucleus with the transcription of the rRNA to subsequent modification and association of several ribosomal and non-ribosomal proteins. The resulting first pre-ribosomal particle is transported into the nucleoplasm and further into the cytoplasm. During this process many factors assemble and get released, whereby one event is a prerequisite for the next. A key step is the association of Drg1 subsequent to the export of pre-ribosomal particles into the cytoplasm. This hexameric AAA-ATPase is the target of diazaborine and catalyses the release of the shuttling factor Rlp24. This reaction is a prerequisite for all following maturation steps.

The structure and assembly of ribosomes is quite well characterised except for its temporal aspects. Thus, the aim of this thesis consisted of the temporal characterisation of the ribosome biogenesis by fluorescence microscopy after diazaborine treatment and its effects on early steps of the pathway. Since the depletion of Rpl40 was reported to cause similar effects like Drg1 inactivation, the role of Rpl40 in cytoplasmic maturation was also investigated by TAP-purification and immunofluorescence.

The temporal analysis of the shuttling factor Bud20 revealed 90% of the fluorescence signal in the nucleus without diazaborine treatment and was reduced to 29% after 5 minutes of incubation in the presence of diazaborine. Nog1 exhibited 83% in the nucleus without treatment and diminished to 29% only after 30 minutes of treatment. The analysis of Nog1 regarding its nucleolar localization yielded 25% of the signal in the nucleolus without diazaborine, which was reduced to 6% after 10 minutes of incubation with the drug. The occurring fragmentation of the nucleolar factor Nop58 was further investigated and revealed its localization within tiny nucleoplasmic spots. The nucleolar factor Noc2 showed the same behaviour as Nop58, in contrast to the nucleolar to nucleoplasmic factor Nsa1. Additionally Noc2 exhibited a higher degree of colocalization with RNA polymerase I after treatment as Nsa1. The analysis of Nop58-TAP particles basically revealed no significant alterations of the particles composition upon treatment with diazaborine. Taken together, these results indicated different surveillance systems and degradation mechanism for particles with different maturation status.

Contents

1 Introduction

Ribosomes are powerful cellular nanomachines transcribing the genetic code of mRNAs in polypeptides. These ribonulceoproteins consist of the large (LSU, 60S) and the small (SSU, 40S) subunit. The large subunit consists of three rRNAs (25S, 5.8S, 5S) and 46 ribosomal proteins whereas the small subunit includes solely one rRNA (18S) and 33 ribosomal proteins (Woolford & Baserga 2013). Since the biogenesis of ribosomes is an essential, highly energy consuming pathway, it requires a significant part of resources in a cell (Warner 1999). For instance all RNA polymerases are involved in this process. RNA polymerase I transcribes the ribosomal RNA (rRNA), RNA polymerase II transcribes the mRNAs required for synthesis of ribosomal proteins and RNA polymerase III transcribes the 5S rRNA. Taken together the transcription required for ribosome biogenesis represents 60% of the total RNA transcription in a cell (Rudra & Warner 2004). Moreover 200 different assembly factors and 76 small nuclear RNAs (snoRNAs) (Warner 1999) are involved in this process that is also linked to other fundamental pathways like cell cycle regulation (Dez & Tollervey 2004). Since ribosome biogenesis is highly conserved in eukaryotes the yeast *Saccharomyces cerevisiae* serves as an excellent model organism due to its easy handling and genetic accessibility (Woolford & Baserga 2013).

1.1 Ribosome biogenesis in general

In yeast, ribosome biogenesis starts in the nucleolus with the transcription of the rDNA (Thiry & Lafontaine 2005) organized in 150 tandem repeats on chromosome XII by RNA polymerase I (French et al. 2003). The resulting 35S rRNA consists of precursors of the SSU rRNA (18S) and the LSU rRNA (25S, 5.8S) separated by internal (ITS) and external (ETS) transcribed spacer. The 5S rRNA of the large subunit is transcribed separately by RNA polymerase III in the opposite direction (Fromont-Racine et al. 2003). Following transcription, many ribosomal proteins and non-ribosomal maturation factors assemble to the rRNA while the obtained 35S rRNA undergoes processing and modification steps (Venema & Tollervey 1999). This is done by maturation factors and snoRNAs, respectively to remove spacer and obtain correct folding (Fromont-Racine et al. 2003; Woolford & Baserga 2013; Venema & Tollervey 1999). For trimming of rRNA ends in the nucleus as well as in the cytoplasm and for snoRNA processing the so-called exosome consisting of different exonucleases is required (van Hoof et al. 2000). One processing step includes the cleavage of the 35S rRNA into the SSU rRNA and the LSU rRNA leading to a separation of further maturation steps (Udem & Warner 1972). Adjacently the particles have to leave the nucleolus and enter the nucleoplasm where they are exported into the cytoplasm. During this journey many factors assemble to the particles and get released in a cascade like way meaning that the release of one factor is the prerequisite for the binding of another (Kappel et al. 2012; Henras et al.

2008). In the cytoplasm final maturation steps are required to gain translational competent ribosomes (Panse & Johnson 2010).

1.2 Nucleolar steps of the ribosome biogenesis

As mentioned before the biogenesis starts with the transcription of the 35S rRNA by RNA polymerase I in the nucleolus. Simultaneously the 5S rRNA is transcribed separately by RNA polymerase III (Fromont-Racine et al. 2003). During ongoing transcription of the 35S rRNA the U3 snoRNA and over 70 factors associate with the nascent rRNA forming the SSU-processome (Figure 1). The SSU-processome includes the U3snoRNP (including Nop58 and Nop1) other modifying snoRNPs (for example t-UTP, Pwp2/UTP-B, UTP-C complex and the Mpp10 and Bms2/Rcl1 subcomplexes) and small subunit ribosomal proteins and is essential for correct cleavage of the rRNA (Dragon et al. 2002; Bernstein et al. 2004; Gallagher et al. 2004; Pérez-Fernández et al. 2007). Following the formation of the SSU processome the initial rRNA processing prior to the separation into pre-60S and pre-40S rRNA (A2-cleavage) occurs co-transcriptionally prior to the disassembly of U3 snoRNA as well as many other associated factors (Tschochner & Hurt 2003). The remaining pre-40S particle includes merely a few non ribosomal factors for instance Enp1, Dim1, Hrr25 and Rrp12 (Tschochner & Hurt 2003) in addition to ribosomal proteins and undergoes solely a few compositional changes prior to export into the nucleoplasm and further into the cytoplasm (Panse & Johnson 2010; Strunk et al. 2012; Kressler et al. 2010). Alternatively the A2- cleavage occurs post-transcriptionally subsequent to the assembly of additional maturation factors forming the 90S particle (Figure 1) (Tschochner & Hurt 2003). Indeed, Kos and Tollervey postulated a co-transcriptional A2-cleavage in 40-70% of the cases (Koš & Tollervey 2010). While the 90S particle consists primarily of SSU r-proteins and 35 non-ribosomal factors mainly required for SSU maturation, components of the pre-60S particles are almost lacking. However, some factors attached to 90S as well as to pre-60S particles like Nop1 and the Rrp5-Noc1-Noc2 complex seem to trigger nascent pre-60S maturation. In addition also other factors like Nop58 are present on pre-60S as well as 90S particles, indicating a role of 90S factors in earliest steps of pre-60S particle formation (Tschochner & Hurt 2003; Hierlmeier et al. 2013). Contrary to pre-40S particles, the following maturation of pre-60S particles is much more complex since 90 trans acting factors are involved in its maturation from the nucleolus to the cytoplasm (Woolford & Baserga 2013). Additionally there are severe changes in the rRNA and protein composition taking place during the maturation process. Thus, after A2-cleavage many ribosomal proteins and a huge number of non-ribosomal assembly factors associate with the particle to form the first pre-60S particle in the nucleolus (Kressler et al. 2010; Fromont-Racine et al. 2003). Prior to the transit into the nucleoplasm the incorporation of the 5S rRNA mediated by Rpf2 and Rrs1 takes place in addition to the exchange of the Noc1-

Noc2 module against the Noc2-Noc3 module thought to have active role in the transition into the nucleoplasm (Kressler et al. 2010).

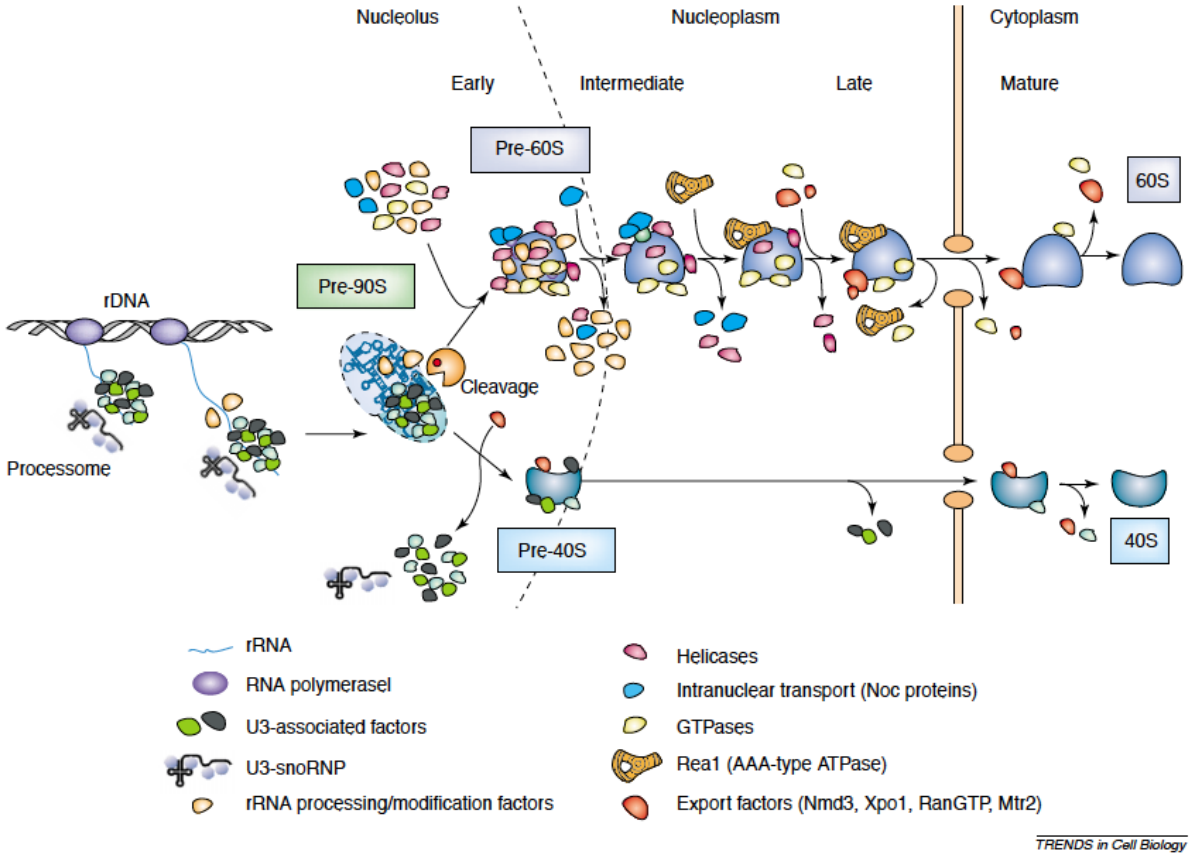

Figure 1: Schematic overview of the ribosome biogenesis emphasizing nuclear steps. The pre-35S rRNA is transcribed by RNA polymerase I prior to the assembly of U3snoRNP, other snoRNPs and SSU r-proteins forming the SSU-processome. Following assembly of additional factors mainly responsible for pre-40S maturation the pre-90S particle is formed. After rRNA cleavage maturation of pre-60S and pre-40S particles occurs separately. The remaining fundamental pre-40S particle undergoes few steps like assembly of a few association factors until the export into the cytoplasm and prior to final cytoplasmic maturation steps. In contrast many r-proteins and association factors assemble to the pre-60S particles and are sequentially released until final maturation steps in the cytoplasm take place. Taken from (Tschochner & Hurt 2003).

1.3 Nucleoplasmic steps and export

Following the nucleolar assembly, the particles are transported into the nucleoplasm, whereby further cleavage of the rRNA takes places. Thereby the help of for instance Nog1, Rlp24 and Tif6 is essential for efficient cleavage (Woolford & Baserga 2013). In the nucleoplasm many assembly factors like Noc2-Noc3 are no longer present and new factors like the Rix1-Ipi1-Ipi3 complex being responsible for final rRNA processing steps, Rsa4, Arx1 and Sda1 associate (Kressler et al. 2010). Subsequent to the nucleoplasmic maturation the mainly hydrophilic pre-60S particles have to pass the hydrophobic meshwork of the nuclear pore complex on their way into the cytoplasm (Woolford & Baserga 2013). The nuclear pore complex is part of the nuclear envelope and represents a barrier from the cytoplasm to the nucleus (Hurt et al. 1999). The lumen is coated with FG-repeat containing nucleoporins

(Woolford & Baserga 2013). As a consequence pre-ribosomal particles have a demand for export factors to cope with this challenge. In addition to the general export machinery including the exportins Crm1/Xpo1, the RanGTPase Gsp1 and several nucleoporins, specific export factors regarding the subunits exist (Hurt et al. 1999; Moy & Silver 1999). However two export factors, namely Rrp12 and Sda1, are required for the export of both subunits (Dez et al. 2006). Pre-60S particles additionally require the export factors Nmd3, Mex67/Mtr2, Arx1, Bud20 and Ecm1, possibly due to their enormous size. Nmd3 harbours a NES (nuclear export sequence) and works as an adapter between the major exportin Crm1 and the pre-ribosomal particles, whereas Mex67/Mtr2, Arx1 and Bud20 bind directly to the particle and the nucleoporins (Yao et al. 2007; Ho et al. 2000; Bassler et al. 2012; Bradatsch et al. 2007; Yao et al. 2010). Pre-40S particles require beside the general export machinery the export factor Ltv1 which is attached to the particles at this maturation stage (Seiser et al. 2006).

Subsequent to the passage through the nuclear pore complex final cytoplasmic maturation steps are required. These include the final processing of the rRNA, the assembly of lacking ribosomal proteins and the release of remaining assembly factors to subsequent recycling into the nucleus (Woolford & Baserga 2013). The cytoplasmic rRNA processing of the pre-40S particles is done by Nob1 while interacting with export factor Ltv1 and the helicase Prp43 (Pertschy et al. 2009). In the cytoplasm the processing of the pre-5.8S rRNA of pre-60S particles has to be completed as well (Woolford & Baserga 2013; van Hoof et al. 2000). Subsequent to accessing the cytoplasm, the AAA-ATPase Drg1 binds to Rlp24 prior to its release and exchange to L24. This event is a prerequisite for all following cytoplasmic maturation events since the inactivation of the temperature sensitive mutant *drg1-18* inhibits the release of all shuttling factors and the assembly of late cytoplasmic association factors in the cytoplasm (Kappel et al. 2012; Pertschy et al. 2007) . Rlp24 acts as a placeholder for L24 and shows a high sequence similarity to L24 despite its C-terminus, required for Drg1 recruitment (Saveanu et al. 2003; Kappel et al. 2012). The incorporated L24 subsequently recruits Rei1 whereby the zinc-finger protein Rei1 enables together with the Hsp70 ATPase Ssa1/Ssa2 and its co-factor Jjj1 the release of the export factor Arx1 (Lebreton et al. 2006; Demoinet et al. 2007; Meyer et al. 2007). The ribosomal protein L12 recruits the phosphatase Yvh1 enabling the exchange of the shuttling factor Mrt4 to the ribosomal protein P0 (Lo et al. 2009; Kemmler et al. 2009). This event is crucial for the formation of the ribosomal “stalk” structure, which is in turn essential for the recruitment and activation of translation factors. Additionally the formation of the “stalk” structure enables the recruitment of the GTPase Elf1 that catalyses together with Sdo1 the release of Tif6. The last maturation steps consists of loading of Rpl10 by its chaperone Sqt1 near Nmd3. Finally Nmd3 and Sqt1 are released (Senger et al. 2001; Menne et al. 2007; Rodríguez-Mateos et al. 2009; Lo et al. 2010; Hedges et al. 2005; West et al. 2005).

1.4 The AAA-ATPase Drg1

The AAA- (ATPases associated with various cellular activities) ATPases belong to a group of phosphate-loop (P-loop) (Erdmann et al., 1991) ATPases. These enzymes use the energy of ATP hydrolysis to remodel their substrates and consist of a N-terminal domain assumed to be the primary target recognition site and two ATPase domains required for nucleotide binding and hydrolysis. However, ATPases fulfil diverse cellular tasks like acting as chaperones, mediating vesicle transport and membrane fusion, protein quality control and proteolysis (Block et al. 1988; Hoskins et al. 1998; Ye et al. 2001; White & Lauring 2007).

Drg1 (diazaborine resistance gene 1) also known as Afg2 (ATPase family gene 2) catalyses the first cytoplasmic maturation step during ribosome biogenesis and belongs to the type II AAA-ATPases. The low abundant protein forms hexamers whereas each protomer consists of a N-terminal domain, two AAA- domains (D1 and D2) and a leucine zipper at the C-terminus with unknown function (Thorsness et al. 1993; Zakalskiy et al. 2002). Since Drg1 exhibits high sequence homology with Cdc48 and its mammalian orthologue p97, a similar functional and structural activity was proposed. The D1 domain of Cdc48 is thereby responsible for oligomerization whereas D2 enables the catalytic activity of this enzyme (Kressler et al. 2012; Kappel et al. 2012). Drg1 exhibits cytoplasmic localization and can be purified with Bud20 or Arx1 containing particles. Inactivation of Drg1 by incubation of a temperature-sensitive mutant at the restrictive temperature leads to an impaired large subunit maturation. This manifests in pre-RNA processing defects and cytoplasmic accumulation of shuttling factors (e.g. Rlp24, Nog1, Bud20, Tif6, Mrt4) and a block in assembly of late joining factors (Sqt1, Rei1) (Pertschy et al. 2007; Bassler et al. 2012; Kappel et al. 2012).

As mentioned before Drg1 is recruited to pre-60S particles by the shuttling factor Rlp24. In more detail the c-terminal domain of Rlp24 and a second domain bind to Drg1 whereas the latter stimulates its ATPase activity. This could also be shown *in vitro* (Kappel et al. 2012; Lo et al. 2010). Rlp24 is supposed to act as a placeholder and shares a high sequence similarity with L24. Indeed, the Drg1 stimulating c-terminal domain is lacking in L24 and the ribosomal protein L24 revealed no impact on Drg1 *in vitro* (Saveanu et al. 2003; Kappel et al. 2012). Additionally a second binding partner namely Nup116 required for the release of Rlp24 was identified via yeast-two-hybrid assays. Since Nup116 is part of the nuclear pore complex this result leads to the assumption that the nucleoporins exerts an up to now unknown role in this release step (Kappel et al. 2012).

1.5 The inhibitor diazaborine and its impact on ribosome biogenesis

The heterocyclic, boron containing compound diazaborine was originally discovered to inhibit enyol-ACP of the fatty acid synthase in gram negative bacteria (Bergler et al. 1994; Grassberger et al. 1984). However, growth inhibition of the yeast *Saccharomyces cerevisiae*

could be observed although no impaired fatty acid synthesis was detectable. Initial studies revealed that diazaborine inhibits rRNA processing due to occurrence of aberrant pre-rRNAs and formation of half-mers (Pertschy et al. 2004). In former studies the AAA-ATPase Drg1 was identified to be the *bona fide* target of this drug (Loibl et al. 2014). Diazaborine binds to Drg1 and blocks its ATP hydrolysis thereby preventing the release of Rlp24. Since this step is a prerequisite of all following cytoplasmic maturation events treatment with this drug leads to impaired pre-60S maturation (Loibl et al. 2014). As a consequence a before mentioned accumulation of shuttling factors in the cytoplasm occurs (Pertschy et al. 2007). Since many of these shuttling factors (e.g Nog1, Rlp24) are essential for nuclear pre-ribosomal maturation steps (Woolford & Baserga 2013), the prevented recycling into the nucleus explains the effect of diazaborine on early steps of the ribosome biogenesis including rRNA processing as described earlier (Pertschy et al. 2004). As already mentioned these defects might lead to aberrant pre-60S particles.

1.6 Surveillance systems for pre-ribosomes

Since ribosome biogenesis constitutes a fundamental, very complex process, failures leads to severe consequences due to accumulation of aberrant ribosomal precursors or defective mature ribosomes (Lafontaine 2010). Thus, cells evolved mechanisms to circumvent those potentially harmful effects. Surveillance systems can be found along the whole maturation pathway (Lafontaine 2010) but this study emphasises on nucle(ol)ar surveillance mechanisms herein referred to as surveillance system. Thereby aberrant rRNAs are poly(A) adenylated by the TRAMP4/5 complexes consisting of the nuclear poly(A) polymerases Trf4 and Trf5, respectively, the putative RNA helicase Mtr4 and two zinc-knuckle proteins Air1p and Air2p. The poly(A) adenylated rRNAs are then degraded by the nuclear exosome (Dez et al. 2006). This nuclease consists of 9 subunits forming a catalytically inactive barrel in addition to Rrp44 exhibiting an exoribonuclease activity. Since the exosome exists in the nucleus as well as in the cytoplasm the nuclear co-factors Rrp6 and Rrp47 confer nuclear specifity (Schuch et al. 2014). This degradation process seems to occur at a specific site in the nucleolus termed “No bodies” (Dez et al. 2006). Recently the recognition of aberrant rRNAs prior to their degradation was identified by Leporé (Leporé & Lafontaine 2011). Thereby aberrant rRNAs or impaired pre-ribosomal particles expose binding sites for the RNA binding Nrd1/Nab3 complex. Adjacently the elongation complex Spt5 which interacts with Rpa190 (large subunit of RNA polymerase I) recruits the Nrd1/Nab complex that in turn interacts with the exosome leading to rRNA degradation (Figure 2) (Leporé & Lafontaine 2011).

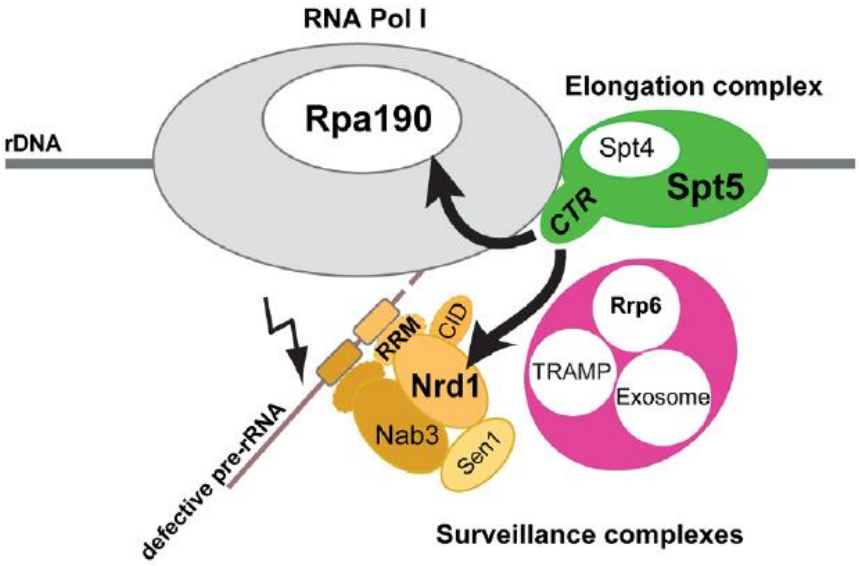

Figure 2: Recognition and degradation of defective pre-rRNAs. In condition of impaired ribosome assembly (misfolded rRNA or delayed assembly of association factors) binding sites for the Nrd1/Nab3 complex are exposed. The elongation complex Spt5 of RNA polymerase I recruits the Nrd1/Nab3 complex which in turn interacts with the exosome leading to degradation. Taken from (Leporé & Lafontaine 2011)

1.7 Aim of this study

The inactivation of Drg1 by its specific inhibitor diazaborine causes an accumulation of shuttling factors in the cytoplasm and as a result, alterations of early steps of the ribosome biogenesis including rRNA processing. To investigate the temporal aspects of the ribosome biogenesis, tagged shuttling protein containing pre-ribosomal particles were followed by fluorescence microscopy after diazaborine treatment. The obtained results could be the starting point of an analysis regarding kinetics of the whole ribosome biogenesis. Additionally the effects of diazaborine on early steps of ribosome biogenesis as a consequence of the nuclear shuttling factor depletion should be investigated by fluorescence microscopy and TAP-purification. Finally, since inactivation of Rpl40 was reported to induce similar defects as inactivation of Drg1, the composition of Arx1 and Bud20 containing particles were analysed after Rpl40 depletion by TAP-purification. This should elucidate the role of Rpl40 in cytoplasmic maturation steps. To investigate the localization of the afore mentioned bait proteins, immunofluorescence upon Rpl40 depletion was performed.

2 Material and methods

2.1 Strains and plasmids

The *S.cerevisiae* strains used in this study are listed in Table 1. The plasmid pFA6a-3mcherry-hphNT1 (see Table 2) used for amplification of the integration cassette for subsequent linear transformation of the received DNA-fragment was propagated in *E.coli* XL-1.

Table 1: *Saccharomyces cerevisiae* strains used in this study

***S.cerevisiae* strain**	**Genotype**	**Source**
Nog1-GFP	*MATα leu2 ura3 his3 met15 NOG1-GFP::HIS3MX6*	Berthold Nobis
Afg2/Tif6-GFP	*MATa leu2 his3 ade2 trp1 ura3 TIF6-GFP::HIS3MX6*	Eva Liebminger
Mrt4-YFP	*MATa his3 ura3 leu2 ade2 trp1 MRT4-GFP::HIS3MX6*	Claudia Schmid
J2_Arx1-TAP	*MATa leu2-3,112 trp1-1 can1-100 ura3-1 ade2-1 his3-11,15 ARX1-TAP::TRP1 rpl40a::KanMX rpl40b::KanMX* [pAS24-*RPL40A*]	Anna Gungl
J2_Bud20-TAP	*MATa leu2-3,112 trp1-1 can1-100 ura3-1 ade2-1 his3-11,15 BUD20-TAP::HIS3MX6 rpl40a: :KanMX rpl40b::KanMX* [pAS24-*RPL40A*]	Anna Gungl
ATCC 201388 (Nop4-GFP)	*MATa his3Δ1 leu2Δ0 met15Δ0 ura3Δ0 NOP4-GFP::HIS3MX6*	Yeast GFP Clone Collection Huh et al., 2003
ATCC 201388 (Noc2-GFP)	*MATa his3Δ1 leu2Δ0 met15Δ0 ura3Δ0 NOC2-GFP::HIS3MX6*	Yeast GFP Clone Collection Huh et al., 2003
ATCC 201388 (Rix1-GFP)	*MATa his3Δ1 leu2Δ0 met15Δ0 ura3Δ0 RIX1-GFP::HIS3MX6*	Yeast GFP Clone Collection Huh et al., 2003
ATCC 201388 (Bud20-GFP)	*MATa his3Δ1 leu2Δ0 met15Δ0 ura3Δ0 BUD20-GFP::HIS3MX6*	Yeast GFP Clone Collection Huh et al., 2003
ATCC 201388 (Nsa1-GFP)	*MATa his3Δ1 leu2Δ0 met15Δ0 ura3Δ0 NSA1-GFP::HIS3MX6*	Yeast GFP Clone Collection Huh et al., 2003
Nog1-GFP Hho1-mCherry	*MATα leu2 ura3 his3 met15 NOG1-GFP::HIS3MX6 HHO1-mCherry::hphNT1*	this study
Nog1-GFP Nop58- mCherry	*MATa his3Δ1 leu2Δ0 met15Δ0 ura3Δ0 NOG1-GFP::HIS3MX6 NOP58-mCherry::hphNT1*	this study
Nog1-GFP Nic96-mCherry	*MATa his3Δ1 leu2Δ0 met15Δ0 ura3Δ0 NOG1-GFP::HIS3MX6 NIC96-mCherry::hphNT1*	this study
Rix1-GFP Hho1-mCherry	*MATa his3Δ1 leu2Δ0 met15Δ0 ura3Δ0 RIX1-GFP::HIS3MX6 HHO1-mCherry::hphNT1*	this study
Rix1-GFP Nic96-mCherry	*MATa his3Δ1 leu2Δ0 met15Δ0 ura3Δ0 RIX1-GFP::HIS3MX6 NIC96-mCherry::hphNT1*	this study
Noc2-GFP Hho1-mCherry	*MATa his3Δ1 leu2Δ0 met15Δ0 ura3Δ0 NOC2-GFP::HIS3MX6 HHO1-mCherry::hphNT1*	this study
Noc2-GFP Nop58-mCherry	*MATa his3Δ1 leu2Δ0 met15Δ0 ura3Δ0 NOC2-GFP::HIS3MX6 NOP58-mCherry::hphNT1*	this study
Noc2-GFP Rpa190-mCherry	*MATa his3Δ1 leu2Δ0 met15Δ0 ura3Δ0 NOC2-GFP::HIS3MX6 RPA190-mCherry::hphNT1*	this study
Nsa1-GFP	*MATa his3Δ1 leu2Δ0 met15Δ0 ura3Δ0 NSA1-GFP::HIS3MX6*	this study

Hho1-mCherry	*HHO1-mCherry::hphNT1*	
Nsa1-GFP **Nop58-mCherry**	*MATa his3Δ1 leu2Δ0 met15Δ0 ura3Δ0 NSA1-GFP::HIS3MX6 NOP58-mCherry::hphNT1*	this study
Nsa1-GFP **Rpa190-mCherry**	*MATa his3Δ1 leu2Δ0 met15Δ0 ura3Δ0 NSA1-GFP::HIS3MX6 RPA190-mCherry::hphNT1*	this study
Bud20-GFP **Hho1-mCherry**	*MATa his3Δ1 leu2Δ0 met15Δ0 ura3Δ0 BUD20-GFP::HIS3MX6 HHO1-mCherry::hphNT1*	this study
Bud20-GFP **Nic96-mCherry**	*MATa his3Δ1 leu2Δ0 met15Δ0 ura3Δ0 BUD20-GFP::HIS3MX6 NIC96-mCherry::hphNT1*	this study
Tif6-GFP **Hho1-mCherry**	*MATa leu2 his3 ade2 trp1 ura3 TIF6-GFP:: HIS3MX6 HHO1-mCherry::hphNT1*	this study
Nop4-GFP **Hho1-mCherry**	*MATa his3Δ1 leu2Δ0 met15Δ0 ura3Δ0 NOP4-GFP::HIS3MX6 HHO1-mCherry::hphNT1*	this study
Mrt4-GFP **Hho1-mCherry**	*MATa his3 ura3 leu2 ade2 trp1 MRT4-GFP::HIS3MX6 HHO1-mCherry::hphNT1*	this study
Nop58-TAP	*MATa ade2 arg4 leu2 ura3 trp1 NOP58-TAP::TRP*	Ed Hurt

Table 2: Plasmids used in this study.

Plasmid	Features	Source
pFA6a-3mcherry-hphNT1	3x mcherry-tag, hphNT1, AmpR	Elmar Schiebel/Stefan Kemmler

2.2 Media and growth conditions

The pFA6a-3mcherry-hphNT1 plasmid harboring *E.coli* Xl-1 was cultivated in 2x TY media containing 100µg/ml ampicillin (Carl Roth GmbH) at 37°C. Yeast strains were grown in complete medium (YPD/YPG) or synthetic dextrose medium (SD) supplied with all amino acids at 30°C (media components and concentrations are listed in Table 3 and amino acid concentrations are listed in Table 4. For agar plates 20g/L agar was added. Transformed strains were cultivated on YPD agar plates containing 400µg/ml hygromycin B (InvivoGen).

Table 3: Compositions of the growth media used for *S.cerevisiae* and *E.coli* strains

Medium	Components	Concentration [g/L]
YPD/YPG	yeast extract	10
	peptone	20
	glucose/galactose	20
SD	YNB	1.4
	$(NH_4)_2SO_4$	5
	Glucose	20
2xTY	peptone	16
	yeast extract	10
	NaCl	5

Table 4: Used 1x amino acid mix for SD media

Aminoacid	Concentration [mg/l]
adenine sulfate	20
Uracil	20
L-tryptophane	20
L-histidine-HCL	20
L-arginine-HCL	20

L-methionine	20
L-tyrosine	30
L-leucine	30
L-isoleucine	30
L-lysine-HCL	30
L-phenylalanine	50
L-glutamic acid	100
L-aspartic acid	100
L-valine	150
L-threonine	200

2.3 Plasmid isolation

The plasmid [pFA6a-3mcherry-hphNT1] was isolated out of *E.coli* Xl-1 via the GeneJET Plasmid Miniprep Kit (Thermo Scientific) and eluted by adding 30µl of ddH_2O from Fresenius.

2.4 PCR

For the amplification of the linear DNA-fragment used for the chromosomal mCherry-tagging of various genes the high fidelity Q5® Polymerase (NEB) in combination with the buffer provided by the supplier was used. The PCR reaction mixture is shown in Table 5. For the used primers see 2.5.

Table 5: Components of the PCR reaction used for generating a linear mCherry-tagging fragment

Component	Final concentration
Template DNA (pFA6a-3mcherry-hphNT1)	1µg
dNTPs	0,25mM
Primer forward	0,4mM
Primer reverse	0,4mM
10x Q5 reaction buffer	1x
DMSO	0.5%
Q5 Polymerase	1U
Final volume	50µl

The PCR was carried out in Veriti 96 Well thermal cycler (Applied Biosystems) using the PCR program that is shown in Table 6.

Table 6: Temperature parameters for the amplification of a linear mCherry- tagging fragment

Temperature [°C]	Time	Cycles
98	1min	1
98	15sec	35
59	1min	
72	4min	
72	10min	1
4	∞	

2.5 Oligonucleotides

The oligonucleotides used in this study were synthesized by Sigma Aldrich. The tagging primers are listed in Table 7. Colony PCR primers for the confirmation of the successful tagging are listed in Table 8.

Table 7: Primers used for the chromosomal mCherry-tagging of the genes *HHO1*, *NOP58*, *RPA190* and *NIC96*

Name	Sequence (5' - 3')	Application
Hho1_S3_fw	AAGGGCCCCTCCGGCATTATTAAACTAAACAAGAAGAAGGTCAAA CTCTCCACGCGTACGCTGCAGGTCGAC	mCherry-tagging of Hho1
Hho1_S2_rv	TTTGATAGTATTGCTATCACCATTGACATTCTCGTTTGGATATTCAC TTTTTAATCGATGAATTCGAGCTCG	
Nop58_S3_fw	GAGAAGAAGGAAAAGAAGTCCAAGAAAGAGAAGAAAGAGAAGAA ACGTACGCTGCAGG TCGAC	mCherry-tagging of Nop58
Nop58_S2_rv	AGGGAACGCGAGGGGTCACTAATTATTAAAATGTAAAATGCATCC atcGATGAATTCGAGCTCG	
Rpa190_S3_fw	GAACAATGTTGGTACGGGTTCATTTGATGTGTTAGCAAAGGTTCC AAATGCGGCTCGTACGCTGCAGGTCGA	mCherry-tagging of Rpa190
Rpa190_S2_rv	TCCTTCAAATAAACTAATATTAAATCGTAATAATTATGGGACCTTTT GCCTGCTTATCGATGAATTCGAGCTCG	
Nic96_S3_fw	GAATGCCAAGGGAAACGTACAGCACTTTAATTAATATAGACGTCT CTCTACGTACGCTGCAGGTCGAC	mCherry-tagging of Nic96
Nic96_S2_rv	GCGCATACTGATATATAGATATAAACAAAAATATACAATATTTAAAA AAAATCGATGAATTCGAGCTCG	

Table 8: Colony PCR Primer used for the confirmation of the correct chromosomal mCherry-tagging

Name	Sequence (5' - 3')
mCherry_colony_fw	CAAGCAACTTTGATTTGTAC
Nop58_colony_fw	TCTCTTGTTGGTCAAGCTAC
Nic96_colony_fw	CGTCAGATTTAGATCAACCATTGGT
S3_colony_rv_neu	ATGTCGACCTGCAGCGTACG
S3_colony_rv	GTCGACCTGCAGCGTACGCG

2.6 Agarose gelelectrophoresis

DNA analysis was carried out in 1% TAE-agarose gels containing 0.15µg/ml ethidium bromide. DNA fragments were separated using a voltage of 6-12V/cm and 1x TAE buffer as running buffer. DNA was visualized by UV-light using a GelDoc™ XR+ (Biorad). Prior to electrophoresis, samples were mixed with 6x loading dye to a final 1x concentration. The compositions of 1xTAE-buffer and 6x loading dye are shown in Table 9.

Table 9: Buffers used for agarose gel electrophoresis for DNA analysis

Buffer	Components	Concentration
1x TAE	Tris/acetate	40mM
	EDTA, pH 8.0	1mM
6x loading dye	Tris-HCL, pH 7.6	10mM
	Xylencyalone FF	0.03%
	Bromphenol blue	0.03%
	Glycerin	60%
	EDTA	60mM

2.7 PCR purification

Prior to the linear transformation in yeast PCR reactions were pooled and purified using the GeneJET Gel Extraction and DNA Cleanup Micro Kit (Thermo Scientific). Elution was carried out using 30µl ddH_2O from Fresenius.

2.8 Yeast transformation

Linear DNA-fragments were transformed into *S. cerevisiae* using the lithium acetate method (Gietz et al. 1995). For the chromosomal tagging 1-10µg purified PCR-fragment (see 2.7) was transformed together with 5µg of single stranded carrier DNA from salmon sperm. Subsequent to the transformation cells were centrifuged and resuspended in 120µl ddH_2O from Fresenius and plated on YPD agar plates. After incubation overnight at 30°C the plates were stamped on YPD agar plates containing 400µg/ml hygromycin B.

2.9 Colony PCR (cPCR)

To confirm the successful chromosomal mCherry-tagging a colony PCR was performed using Taq Polymerase and ThermoPol® buffer (NEB). For the cPCR cells were resuspended in 20µl ddH_2O (Fresenius) and incubated for 10 minutes at 95°C. After centrifugation the received supernatant was used as template. The used primers are listed in Table 8. The PCR reaction mixture is shown in Table 10 and the temperature profile in Table 11.

Table 10: PCR reaction compounds used for the confirmation of the correct chromosomal mCherry-tagging

Compound	Concentration
10x ThermoPol® Reaction buffer	1x
dNTPs	0,25mM
Primer forward	1mM
Primer reversed	1mM
Taq polymerase	2,5U
Supernatant	7,5µl
Final volume	20µl

Table 11: Used temperature parameters for the colony PCR to confirm correct chromosomal mCherry-tagging

Temperature [°C]	Time [min]	Cycles
95	5	1
95	1	35
55	1	
72	1	
72	5	1
4	∞	1

2.10 Tandem affinity purification (TAP)

2.10.1 Growth conditions for J2_Bud20-TAP and J2_Arx1-TAP

For the TAP- purification 4 liters of each strain were grown in YPG at 30°C and 110rpm overnight to an OD_{600} of 0.3-0.4. The cells were harvested in sterile 0,5l centrifugation tubes (Beckman Coulter™ centrifuge, rotor JA-10) for 5 minutes at 5000rpm and room temperature. Half of the cell pellets were resuspended in YPD and YPG, respectively to subsequent incubation for 4 hours at 30°C and 110rpm. Prior to harvesting the optical density was measured and the cells were harvested in non-sterile 1l centrifugation tubes buy centrifugation for 5 minutes at 5000rpm and 4°C (Beckman Coulter™ centrifuge, rotor JLA-8.1000). The cell pellets were washed with ice-cold water, transferred in a 50ml falcon tube and centrifuged for 5 minutes at 4000rpm and 4°C (Eppendorf Centrifuge 5804 R). Finally the cell pellets were stored at -80°C until usage.

2.10.2 Isolation of pre-ribosomal particles (TEV-eluate)

In this study solely the first purification step of the TAP-purification protocol was performed to gain the TEV-eluate. Used buffers are listed in Table 12. The frozen cell pellets were defrosted subsequent to the addition of an equal amount of lysis buffer A. Cells were broken using a CO_2 cooled Braun's Desintegrator (MSK Homogenisator, B. Braun Biotech) for 4 minutes subsequent to the addition of 1.5 fold volumes of glass beads. Crude extracts (CE) were received by successive centrifugation steps at 4°C at 5000rpm (5 minutes) (Eppendorf Centrifuge 5804 R), 19000rpm (15min) and 19000 rpm (30 minutes) (Beckman Coulter™ centrifuge, rotor JA-25.50) and aliquots for subsequent SDS-PAGE were stored at -20°C. IgG sepharose beads (GE Healthcare) were equilibrated by washing twice with buffer A at 4°C. Crude extracts were incubated with IgG-sepharose beads (1000µl per liter culture) for 90 minutes on a rotating wheel at 12 rpm and 4°C. Subsequent to centrifugation aliquots of the supernatants were stored at -20°C and the remaining beads were washed twice with buffer A containing 1mM DTT and once with TEV-cleavage buffer. For TEV-cleavage the sepharose IgG beads were incubated with 10µl TEV-protease and 80µl TEV-cleavage buffer at room temperature on a rotating wheel at 12 rpm for 60 minutes. After centrifugation at

4000 rpm and 4°C for 3 minutes (tabletop centrifuge) the supernatant was divided into aliquots and 5x FSB buffer was added to a final concentration of 2.5x. The received TEV-eluates were stored at -20°C until the investigation by SDS- PAGE and western blot.

Table 12: Composition of buffers used for tandem affinity purifications

Buffer	Components
Buffer A	20mM HEPES/NaOH, pH 7.5 10mM KCL 2.5mM $MgCl_2$ 1mM EGTA pH 7.5
Lysis buffer A	Buffer A+ 0.5mM PMSF (Sigma Aldrich) 1mM DTT 2x Protease inhibitor Complete® (Roche)
TEV- cleavage buffer	Buffer A+ 100mM NaCl 0.5mM DTT

2.10.3 Growth conditions for Nop58-TAP harboring strains

For the Nop58 tandem affinity purification 6l of YPD were inoculated with Nop58-TAP harboring strains and cultivated overnight at 30°C and 110rpm to an OD_{600} of 1.0-1.2. Diazaborine (100µg/ml) was added and the cells were harvested after 5, 15, 30 and 60 minutes of diazaborine (Novartis) treatment and without diazaborine treatment by centrifugation for 2 minutes at 5000rpm and 4°C (Beckman Coulter™ centrifuge, rotor JLA-8.1000). The cell pellets were washed with ice-cold water containing 100µg/ml diazaborine (alternatively without dazaborine for the pellet without diazaborine treatment) and stored at -20°C until usage.

2.10.4 Tandem affinity purification using magnetic beads

For the TAP- purification see 2.10.2. For the tandem affinity purification with magnetic beads (BCMag™ Epoxy-Activated Magnetic Beads Bioclone coupled with rabbit IgG Dunn Labortechnik kindly provided by Gertrude Zisser) 150µl magnetic beads per liter culture were applied. Instead of centrifugation, beads were removed by using a magnetic rack. The magnetic beads were washed 3 times with buffer A prior to protein binding. Nop58-TAP was eluted by addition of 125µl TEV- cleavage buffer and 10µl TEV protease.

2.10.5 SDS- PAGE

Protein samples containing 2.5x FSB buffer (0.3M Tris-HCL, pH 6.8, 12% SDS, 25% β-mercapto ethanol, 40% glycerol and 0.02% bromophenol blue) were incubated at 95°C for 10 minutes and loaded onto a Novex® NuPAGE® Bis-Tris gradient gel (4-12%) (Life Technologies). Proteins were separated using a Novex® NuPAGE® SDS-PAGE gel electrophoresis system (Life Technologies) containing 1x NuPAGE® MOPS SDS running

buffer (Life Technologies). PageRuler™ Prestained Protein Ladder or unstained protein molecular weight marker from Thermo Scientific served as molecular weight standard.

2.10.6 Western Blot

Protein samples were separated via SDS-PAGE (see 2.10.5) and blotted on a PVDF membrane (Carl Roth GmbH) using the tank-blot-system TE22 Mighty Small™ Transphor Unit (Hoefer). The transfer was carried out in CAPS-buffer (10mM CAPS, pH 11.0, 10% methanol) for 2 hours at 220mA. To prevent unspecific binding of the antibodies the membrane was blocked with 0.5% milk powder in 1x TST (1.5M NaCl, 1% Tween 20, 0.5M Tris/HCl pH 7.5) overnight at 4°C. Alternatively the blocking was performed by incubating the membrane in 3% milk powder in 1xTST for 15 minutes at room temperature. After blocking the membranes were incubated with the primary antibody (diluted in 1% milk powder in 1xTST) for 1 hour and washed 3 times with 1x TST for 5 minutes. The membrane was incubated with a HRP- conjugated secondary antibody (α-rabbit POX from goat, diluted 1:15,000 in 1% milk powder in 1xTST) and washed 3 times for 5 minutes with 1x TST. All washing and incubation steps were performed on a platform of agitation at room temperature except the overnight blocking step which was performed at 4°C. After the washing steps membranes were incubated with Amersham ECL Western Blotting Detection Reagent (GE Healthcare) and chemiluminescence signals were detected by use of x-ray films. Alternatively detection was performed by incubating the membranes with Clarity™ Western ECL Substrate and using the ChemiDoc™ Touch Imaging System (both BioRad®). To remove bound antibodies the membrane was incubated with stripping solution (60mM Tris-HCL, pH 6.8, 2% SDS, 100mM β-mercapto ethanol) for 15 up to 30 minutes at 50°C in a shaking water bath. The membranes were reused for detection with other primary and secondary antibodies or dried for storage subsequent to 3 washing steps with 1x TST for 5 minutes. All antibodies used in this study were raised in rabbits and are listed in Table 13.

Table 13: Polyclonal primary antibodies raised in rabbit used in this study. α-HA was conjugated to HRP.

Antibody	Protein size [kDA]	Dilution	Source
α-Cbp	variable	1:2000	Milipore
α-Drg1	84.7	1:7500	IMB
α-Mex67	67.4	1:10000	E. Hurt
α-Nmd3	59.1	1:4000	A. Johnson
α-Noc1	116.0	1:5000	P. Milkereit
α-Noc2	81.0	1:5000	P. Milkereit
α-Noc3	75.0	1:5000	P. Milkereit
α-Nog1	74.4	1:5000	M. Fromont-Racine
α-Nop1	34.0	1:3000	E. Hurt
α-Nop4	78.0	1:5000	IMB
α-Nop7	69.9	1:20000	E. Hurt
α-Nsa2	29.8	1:5000	M. Fromont-Racine

α-Rei1	45.9	1:5000	M. Fromont-Racine
α-Rlp24	23.9	1:2500	M. Fromont-Racine
α-Rsa4	57.0	1:15000	E. Hurt
α-Rpl10	25.4	1:2000	B.L. Trumpower
α-Rpl16	22.2	1:30000	S. Rospert
α-Rrp12	137.0	1:5000	M. Dosil
α-HA (Rpl40)	25.0	1:6000	Roche
α-Arp3	50.0	1:1000	Santa Cruz Biotechnology
α-Sqt1	47.1	1:1000	B.L. Trumpower
α-A135	135.7	1:2000	M. Oakes
α-Ubiquitin	variable	1:1000	A. Bachmair
α-GAPDH	35.6	1:40000	TU Graz

2.10.7 Coomassie staining and colloidal staining

NuPAGE® gels were stained with Coomassie solution (0.25% Coomassie Brilliant Blue, 10% acetic acid, 45% ethanol) for 30 minutes, destained with a solution containing 10% acetic acid and 40% ethanol and fixed in 3% acetic acid. Alternatively gels were stained using Novex® colloidal blue staining kit (Life Technologies).

2.10.8 Determination of protein concentrations

Protein concentrations were determined by the use of Bradford method. The required Bradford reagent was received from BioRad®. All measurements were carried out in triplicates according to the method recommended by the manufacturer. Bovine serum albumin (Boerhinger Mannheim) was taken for generation of the protein standard.

2.11 Microscopy

2.11.1 Immunofluorescence

Table 14 Buffers and solutions used for immunofluorescence

Buffers and solutions	Components
IF- buffer A	100mM KPO_4 buffer, pH 7.5 1.2M sorbitol
IF- buffer B	100mM Tris/HCL, pH 7.5 150mM NaCl 0.1% Triton X-100
1x PBS pH 7.4	100mM Na_2HPO_4 20mM K_2HPO_4 137mM NaCl 27mM KCl

Used buffers and solutions are listed in Table 14. To localize Bud20-TAP and Arx1-TAP, respectively before and after depletion of Rpl40 an immunofluorescence was performed. Cells were grown under the same conditions as described for tandem affinity purification (see 2.10.1) with the only exception that the culture volume was solely 50ml per strain and cells were harvested by centrifugation at 3500rpm for 5 minutes. After 4 hours of glucose

depletion the cells were fixed by adding 1/10 culture volume of a 1:1 solution of 1M potassium permanganate pH 7 and formaldehyde (37%) directly into the culture medium and incubation for 10 minutes at room temperature. Cells were harvested by centrifugation at 1800rpm and room temperature for 5 minutes, subsequently resuspended in 0,1M KPO_4 buffer containing 4% formaldehyde and incubated for 1 hour at room temperature and gentle shaking. The fixation process was stopped by addition of 1M Tris/HCl pH 7.5 to a final concentration of 50mM. The cells were harvested and washed 3 times with 1ml IF-buffer A. Fixed cells were spheroplasted using 50µg zymolyase in IF-buffer A containing 30mM β-mercapto ethanol at room temperature for 80 up to 120 minutes. Spheroplasts were washed twice with IF-buffer A and adhered to poly-L-lysine coated slides (Thermo Scientific) for 30 minutes at room temperature. Adhered cells were washed once with ddH_2O and air dried to subsequent permeabilisation with IF-buffer B containing 0.1% triton X-100 for 30 minutes at room temperature. After cells were washed 3 times with IF-buffer B containing 0.1% triton X-100 unspecific binding sites were blocked using 1%BSA in 1x PBS for 30 minutes at room temperature. Cells were incubated with the primary antibody (α-protein A, 1:1500 diluted in 1% BSA in 1x PBS) for 1 hour at room temperature and washed 3 times with 1% BSA in 1x PBS. Subsequent to the incubation with the secondary antibody (goat-α-rabbit rhodamine conjugated, 1:200 diluted in 1% BSA in 1x PBS) for 1 hour at room temperature in the dark, cells were washed 5 times with 1% BSA in 1x PBS and once with 1x PBS at room temperature. DAPI (4', 6'- diamidino-2-phenylindole) staining was performed by adding 1µg/ml DAPI solution (in 1xPBS) and incubating for 15 minutes in the dark at room temperature. Cells were washed 3 times with 1x PBS at room temperature and 3µl Kaiser's gelatin was added on each well of the slide and finally covered with a cover slide. The slides were stored at 4°C until usage.

2.11.2 Confocal laser scanning microscopy

Imaging was performed using a Leica SP5 confocal microscope (Leica Mannheim) with spectral detection and a HCX PL APO 63x/NA1.4 oil immersion objective. Fluorescence signal was detected using a sensitive hybrid photon-detector (Leica Mannheim). GFP was excited at 488nm, emission detected between 500-550nm. mRFP was excited at 561nm and emission detected between 570-650nm. Fluorescence and transmission images were acquired simultaneously. Z-stacks were recorded using a sampling rate of 100x100x250nm.

2.11.2.1 Diazaborine treatment of GFP/mCherry-tagged strains

For the standard procedure strains were grown to an OD_{600} 0.45 in a culture volume of 10ml SD-medium (supplemented with all amino acids). Diazaborine was added to the cell culture to a final concentration of 10µg/ml and cells present in the culture were harvested after 0, 2, 5, 10, 15 and 30 minutes of diazaborine treatment. The pellet was applied on 2% agar slides

containing SD media (supplemented with all amino acids and additionally 100µg/ml diazaborine). As a negative control untreated cells were applied on agar coated slides supplied with all amino acids but without diazaborine. The cells were examined via microscopy using a slice thickness of 0.25µm.

2.11.3 Image processing

Image processing and colocalization analysis were performed using the open-source software Fiji (Schindelin et al. 2012). 3D raw data were filtered using 3D Gaussian filter (kernel size 1x1x1). Subsequent to filtering the mCherry-images were thresholded using the automatic threshold yen algorithm. The binary pictures were closed using 2 iterations to subsequent filling of remaining holes. Adjacently regions of interests were created by the command “analyze particles”. The raw intensity of the nuclear signal was measured by the use of the afore created mask. Following the analysis the created regions of interests were filled black and the received picture was thresholded using the automatic threshold triangle (in case of Nog1) and yen (in case of Bud20) algorithm. The created mask was used for the analysis of the cytoplasmic intensity.

2.11.4 Fluorescence microscopy

Fluorescence microscopy was performed using an Axioskop (Zeiss) equipped with a narrowband filter for eGFP (Zeiss). Pictures were taken using 40x lens and 1.6x secondary magnification. For phase contrast pictures an exposure time of 100ms was chosen. For GFP pictures an exposure time of 4000ms was chosen and for mCherry pictures 2000ms. For cell preparation see 2.11.2.1.

2.11.5 GFP quantification

For the GFP quantification a standard curve was generated by the use of purified hexahistidine GFP (kindly provided by Gertrude Zisser). Cells exhibiting an OD_{600} of 0.5-0.8 were mixed with GFP solutions containing different concentrations and pictures were taken as described in 2.11.2.

3 Results

3.1 Effect of diazaborine on the localization of pre-60S particles

3.1.1 Generation of a semi-automated quantification system

Diazaborine, a specific inhibitor of the ribosome biogenesis is known to block the first cytoplasmic maturation step. This consists of the binding of Drg1 to the newly exported pre-60S particle in the cytoplasm and the subsequent release of Rlp24. The inhibition of this step leads to an accumulation of many shuttling factors in the cytoplasm and further to alterations in the compositions of nucle(ol)ar particles ((Loibl et al. 2014; Pertschy et al. 2007) Isabella Klein and Gertrude Zisser, unpublished data). We wanted to investigate the alterations in pre-60S localization upon diazaborine treatment in a temporal manner by fluorescence microscopy. For this purpose a semi-automated quantification method should be established.

3.1.1.1 Optimization of treatment conditions

For the first approach a GFP tagged version of the shuttling factor Nog1 was taken and additionally Hho1 of *Saccharomyces cerevisiae* was tagged with mCherry to mark the nucleoplasm. Cells on agar slides containing SD media supplied with all amino acids and 100µg/ml diazaborine were investigated by fluorescence microscopy. As a negative control cells were investigated on agar slides containing SD media supplied with all amino acids without diazaborine. As a positive control cells were grown in liquid SD media supplied with all amino acids and 10µg/ml diazaborine and investigated on slides coated with agar supplied with SD media, all amino acids and 100µg/ml diazaborine.

The shuttling factor Nog1-GFP entered the cytoplasm initially after 2 minutes of diazaborine treatment. In contrast to the positive control showing a complete depletion of Nog1 in the nucleoplasm after 30 minutes of diazaborine treatment the cells incubated on agar slides showed still a high GFP signal remaining in the nucleus after 30 minutes of diazaborine treatment (Figure 4). Because of the strong dissimilarities of the behavior of Nog1 upon diazaborine treatment between liquid culture and cells merely treated on agar, the treatment in liquid culture was chosen for further experiments. Hence cells were taken out of a liquid culture subsequent to different times of treatment with 10µg/ml diazaborine and investigated by fluorescence microscopy on agar slides containing SD media and 100µg/ml diazaborine.

3.1.1.2 Selection of suitable shuttling factors and a nuclear marker

For the further establishment of the quantification method the selection of suitable shuttling factors was required (Figure 7). Hence, two other shuttling factors Mrt4-GFP and Tif6-GFP (herein referred to as Mrt4 and Tif6) already known to show a cytoplasmic accumulation with

some inclusion bodies remaining in the nucleus after diazaborine treatment (Diplomarbeit Claudia Schmidt) were used. As a control the strictly nucleoplasmic maturation factor Rix1-GFP was investigated (herein referred to as Rix1).

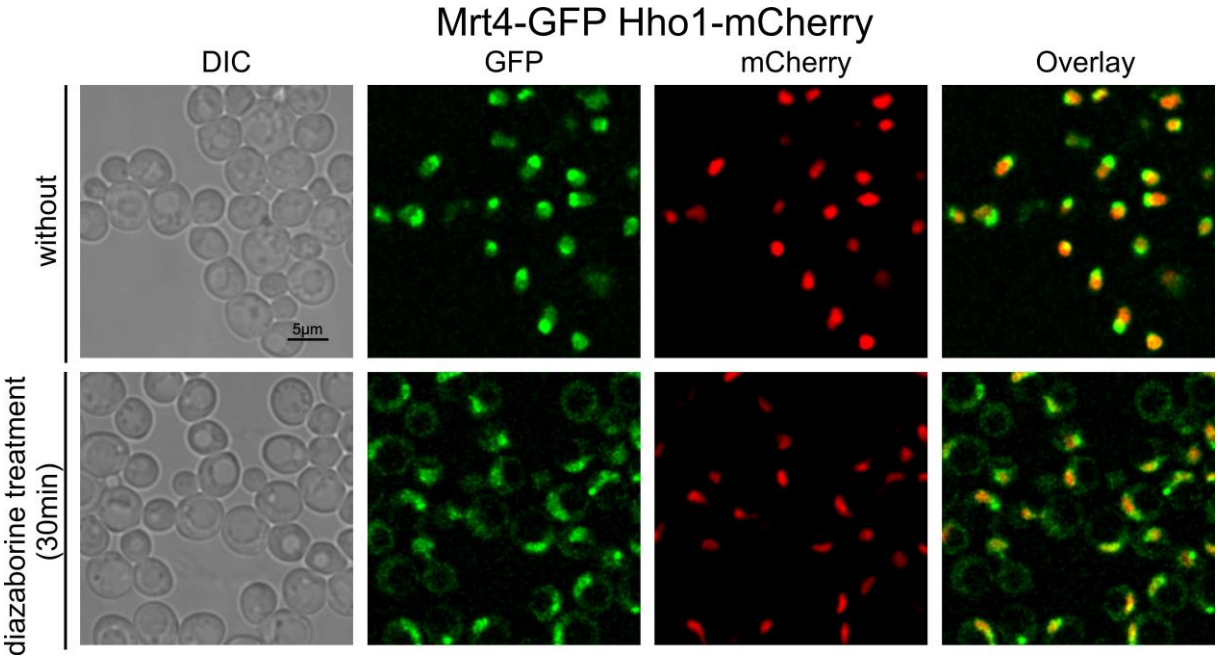

Figure 3: Mrt4 does not show a complete nuclear depletion after 30 minutes of diazaborine treatment. Cells were grown and treated according to the standard procedure depicted in 2.11.2.1. The nucleoplasm was marked by Hho1. Mrt4 showed nucleolar to nuclear localization without diazaborine treatment and slightly entered the cytoplasm after treatment with diazaborine after 30 minutes.

Without diazaborine inhibition Mrt4 showed a mainly nucleolar to slightly nucleoplasmic localization. Upon 30 minutes of diazaborine treatment Mrt4 showed a higher signal in the nucleoplasm as well as in the cytoplasm. Additionally the nucleoplasm was not completely depleted and showed some tiny spots as expected from the results of Claudia Schmidt (Figure 3). The shuttling factor Tif6 showed like Mrt4 a mainly nucleolar to slight nucleoplasmic localization. But in contrast to Mrt4 some very small accumulation spots occurred in the nucle(ol)us in the absence of the inhibitor and after 5 minutes of diazaborine treatment. As expected also Tif6 did not show a complete depletion of the nucleus after the whole period of treatment with diazaborine. However the nuclear signal shifted from the nucleolus into the nucleoplasm after the whole treatment (Figure 8). An enlarged version of the microscopy pictures of Tif6 and Mrt4 without and upon 30 minutes of diazaborine treatment is shown in Figure 14. The nucleoplasmic maturation factor Rix1 remained in the nucleus over the whole period of treatment (Figure 5).

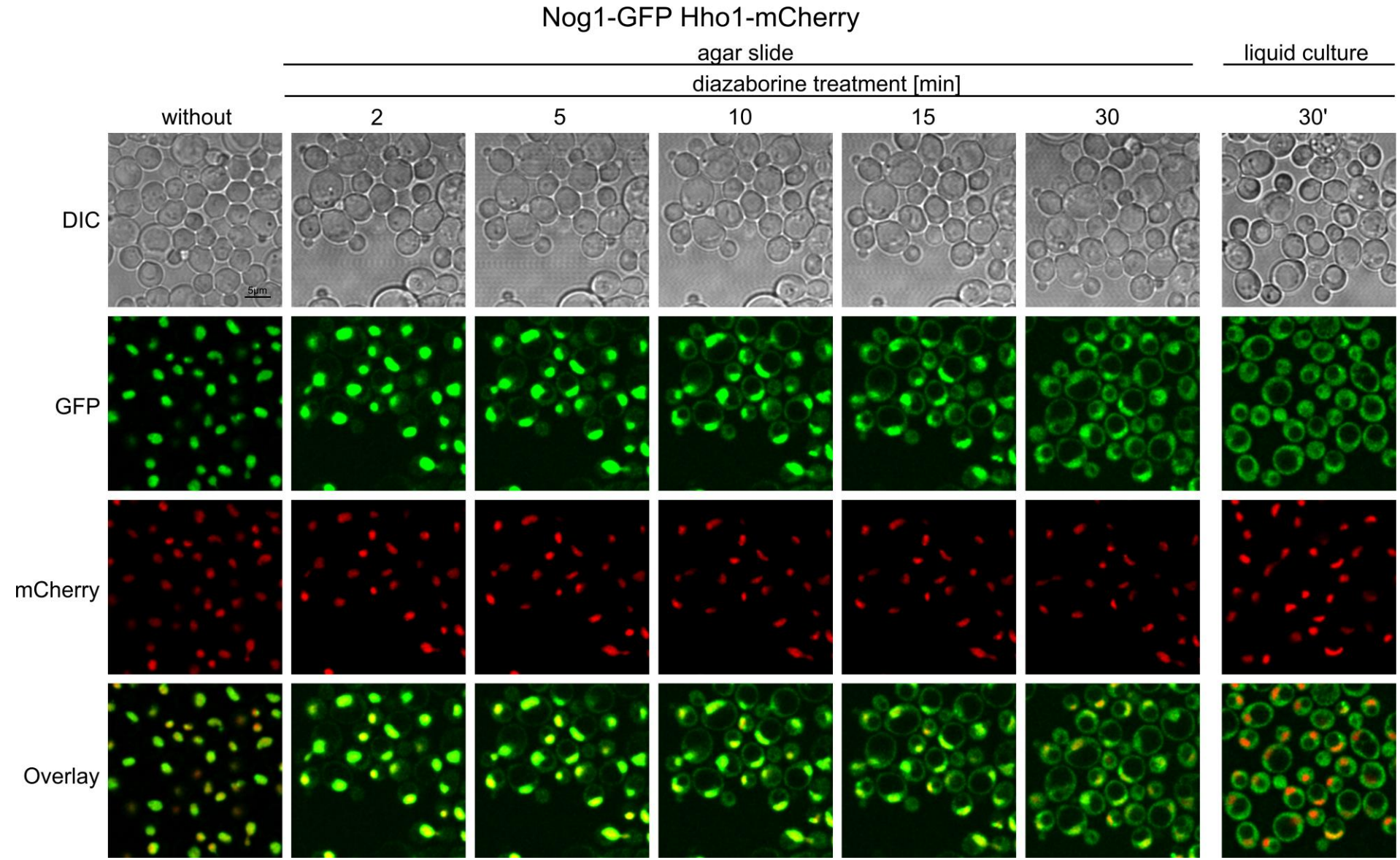
Nog1-GFP Hho1-mCherry
agar slide
liquid culture
diazaborine treatment [min]
without
2
5
10
15
30
30'
DIC
GFP
mCherry
Overlay
5µm

Figure 4: Comparison of Nog1 cytoplasmic accumulation after diazaborine treatment on agar slides and in liquid culture. Cells were grown to an OD_{600} of 0.4-0.5 and applied on agar slides supplied with all amino acids and 100µg/ml diazaborine. As a negative control cells were applied on the same slides without diazaborine and as a positive control cells were supplied with 10µg/ml diazaborine directly in the liquid culture and applied on diazaborine containing agar slides. Pictures were taken after the indicated periods of treatment. Nog1 initially located in the nucleolus and the nucleoplasm. After 30 minutes of treatment a strong cytoplasmic signal was detectable. In contrast to the liquid control, a portion of the signal of Nog1 was detectable also after 30 minutes in the nucleus.

The quantification of the obtained data revealed that the area flanked by Hho1 (histone 1) did not fully cover the whole nucleoplasm. Referred to the Hho1-mCherry signal marking the nucleoplasm, the quantification yielded 70% of Rix1 in the nucleus (Figure 6). Since Rix1 is strictly located in the nucleoplasm this result seemed very unlikely. Additionally this problem could be observed on the overlay whereby the green Rix1 signal surrounds the orange additive signal of Rix1 (green) and Hho1 (red), respectively (Figure 5). For further analysis Nic96 was mCherry tagged since it is a protein being part of the nuclear envelope and thus should cover the whole nucleus. Referred to the Nic96-mCherry signal as nuclear marker approximately 90% of Rix1 located in the nucleus (Figure 6).

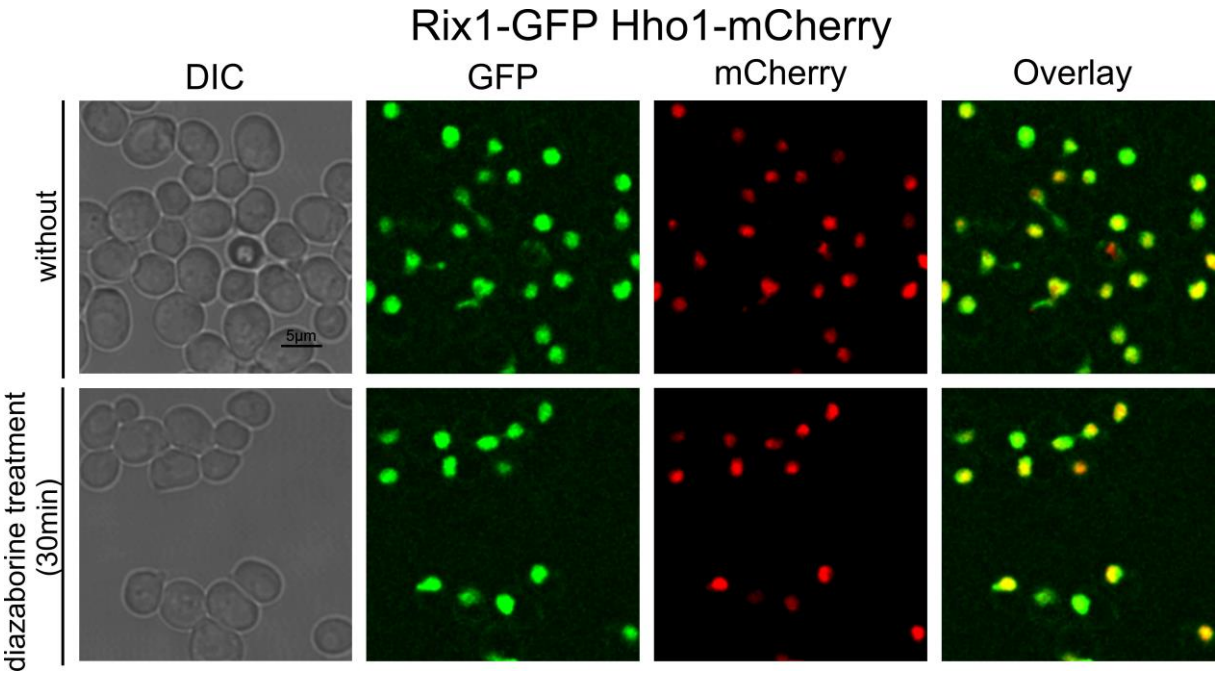

Figure 5: Localization of the nucleoplasmic factor Rix1 remains unchanged after 30 minutes of diazaborine treatment. Cells were grown and treated according to the standard procedure depicted in 2.11.2.1. Hho1 served as nucleoplasmic marker. Rix1 showed in the presence and absence of diazaborine nucleoplasmic localization.

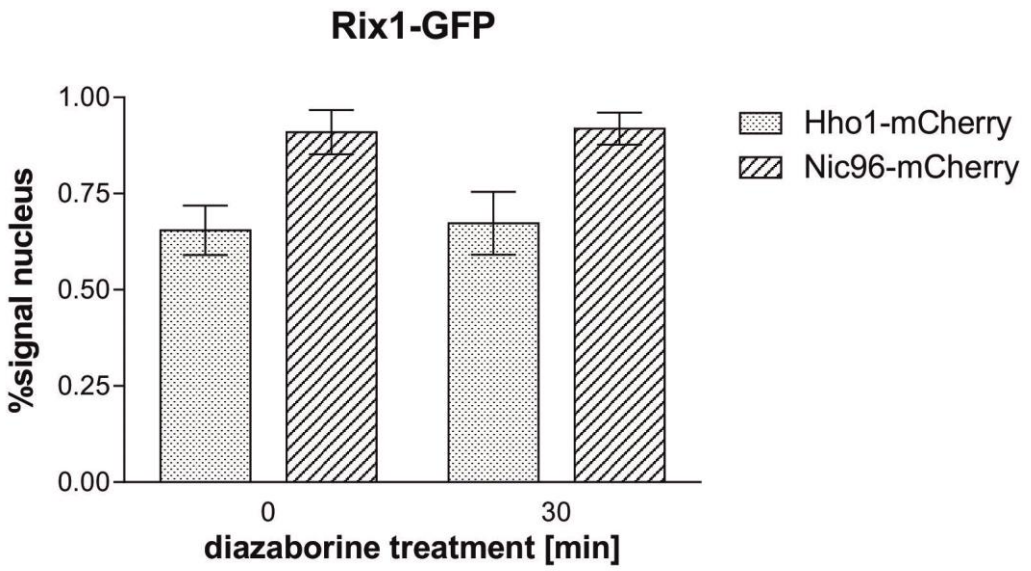

Figure 6: Quantification of Rix1 colocalization with Hho1-mCherry or Nic96-mCherry. The signals were obtained by creating regions of interests of the mCherry signal and measuring the GFP signal of Rix1 in the corresponding area. Means and standard deviations were obtained by the calculation of triplicates.

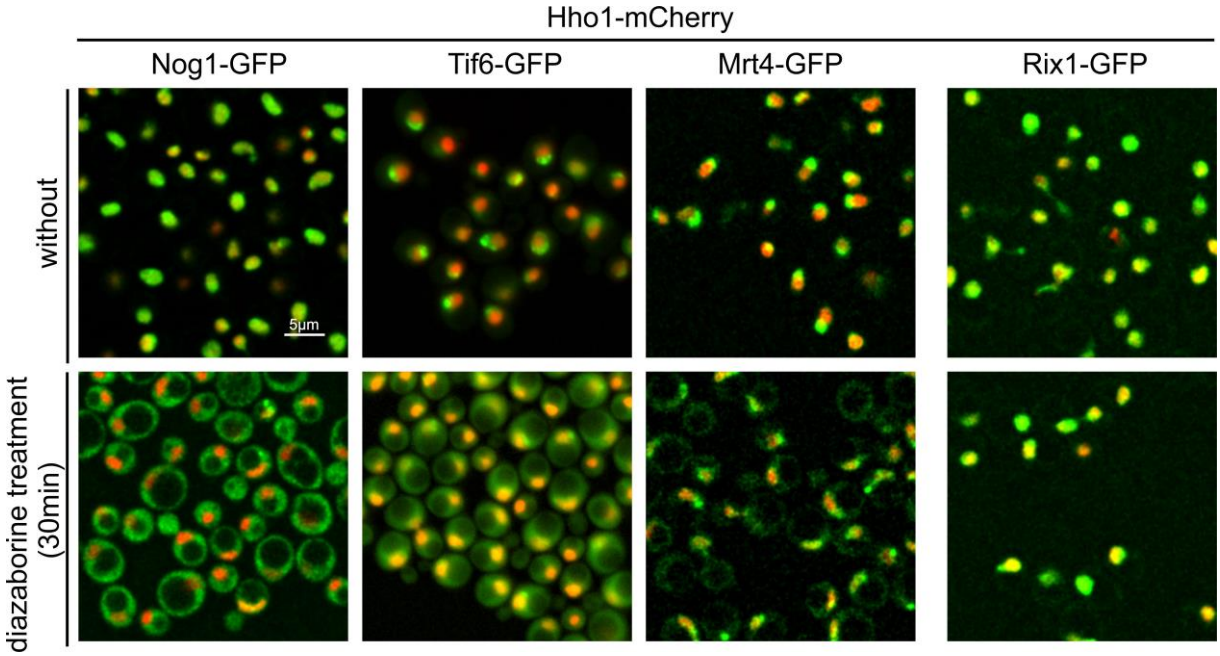

Figure 7: Selection of suitable shuttling factors for kinetic measurements of pre-60S maturation. Cells were grown and treated according to the standard procedure depicted in 2.11.2.1. Pictures were taken after the indicated periods of time (using the Axioskop in case of Tif6). Hho1 marked the nucleoplasm. All tested shuttling factors showed a nuclear localization in the absence of the inhibitor. After 30 minutes of treatment with diazaborine Tif6, Mrt4 and Nog1 accumulated in the cytoplasm. In contrast to Nog1 a remaining GFP signal in the nucleus was detectable for Tif6 and Mrt4.

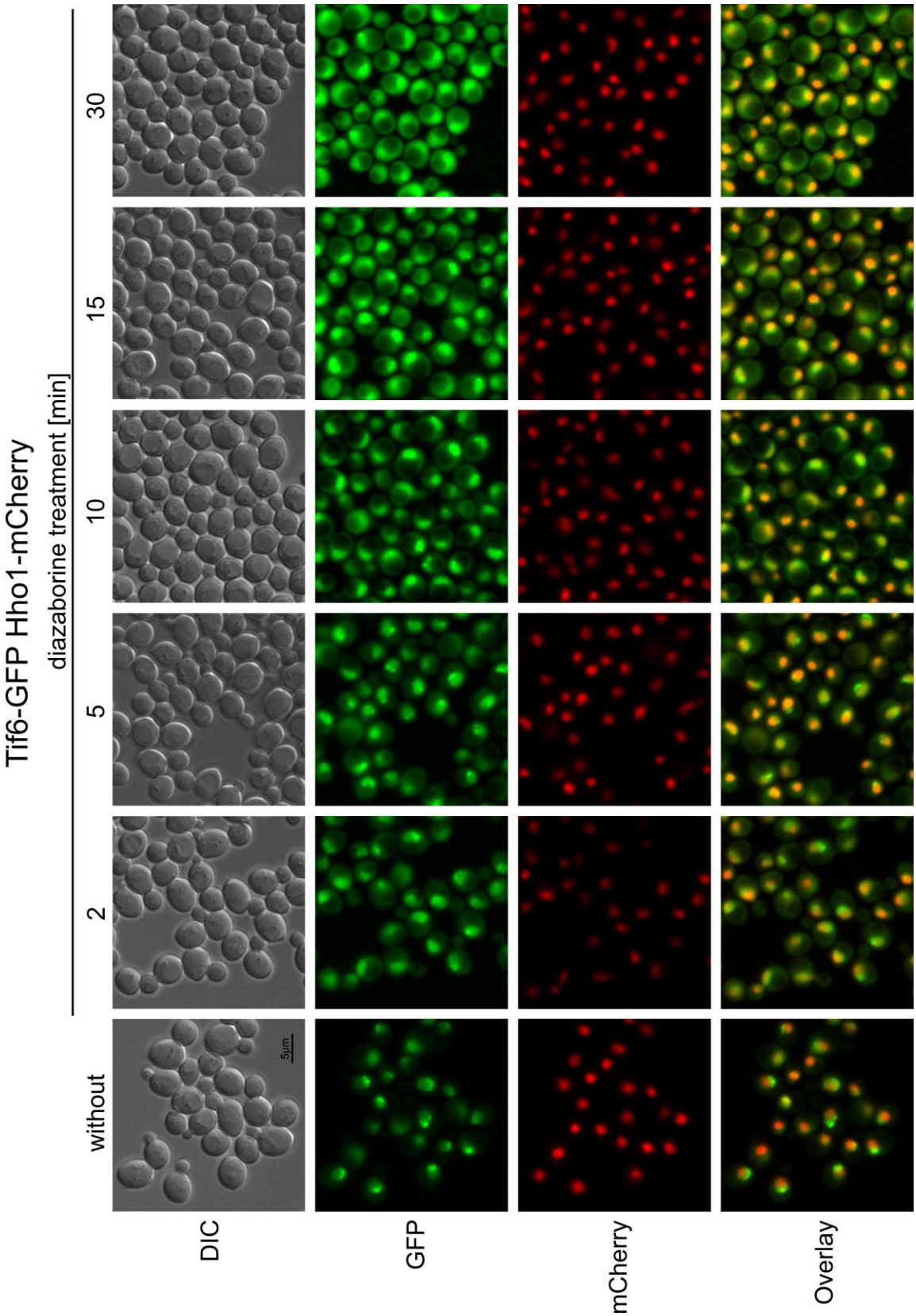

Figure 8: Tif6 does not show a complete nuclear depletion after 30 minutes of diazaborine treatment. Cells were grown and treated according to the standard procedure depicted in 2.11.2.1. Pictures were taken after the indicated periods of time using the Axioskop fluorescence microscope. Hho1 marked the nucleoplasm. Tif6 showed an initial localization in the nucleolus and the nucleoplasm. After 2 minutes of treatment Tif6 started to accumulate in the cytoplasm. After 30 minutes a strong cytoplasmic accumulation was visible. A remaining nuclear signal was detectable though.

3.1.1.3 Semi-automated quantification of GFP intensities and GFP quantification

The selection of suitable shuttling proteins revealed Nog1 as proper candidate due to its complete nuclear depletion after 30 minutes of diazaborine treatment (Figure 7). To gain some insights into the kinetics of late nuclear particles as well, the shuttling factor Bud20 was selected.

Strains containing a GFP tagged version of the shuttling proteins Nog1, Bud20 and again as a control the nucleoplasmic maturation factor Rix1 each expressing Nic96-mCherry fusion were taken for the following fluorescence microscopy. These results served as a basis for the subsequent quantification of the localization of the received GFP signal. Therefore cells were treated with 10µg/ml diazaborine in a liquid culture and applied on agar coated slides containing all amino acids and 100µg/ml diazaborine. For the subsequent quantification the Nic96-mCherry area was determined by setting an automatic threshold and creating a binary mask prior to creating regions of interests using the freeware program Fiji (Schindelin et al. 2012). The amount of the whole GFP signal locating in the afore created regions of interests was measured and the areas were filled to exclude them for further evaluation. The remaining area of the GFP-signal was determined by setting a threshold and creating a binary mask prior to creating regions of interests again. The amount of the GFP-signal was measured in these created regions of interest. To quantify the ratio between the signal in the nucleus and the surrounding cytoplasm the “raw intensity” of the measured pixels was used. The experiment was carried out independently 3 times.

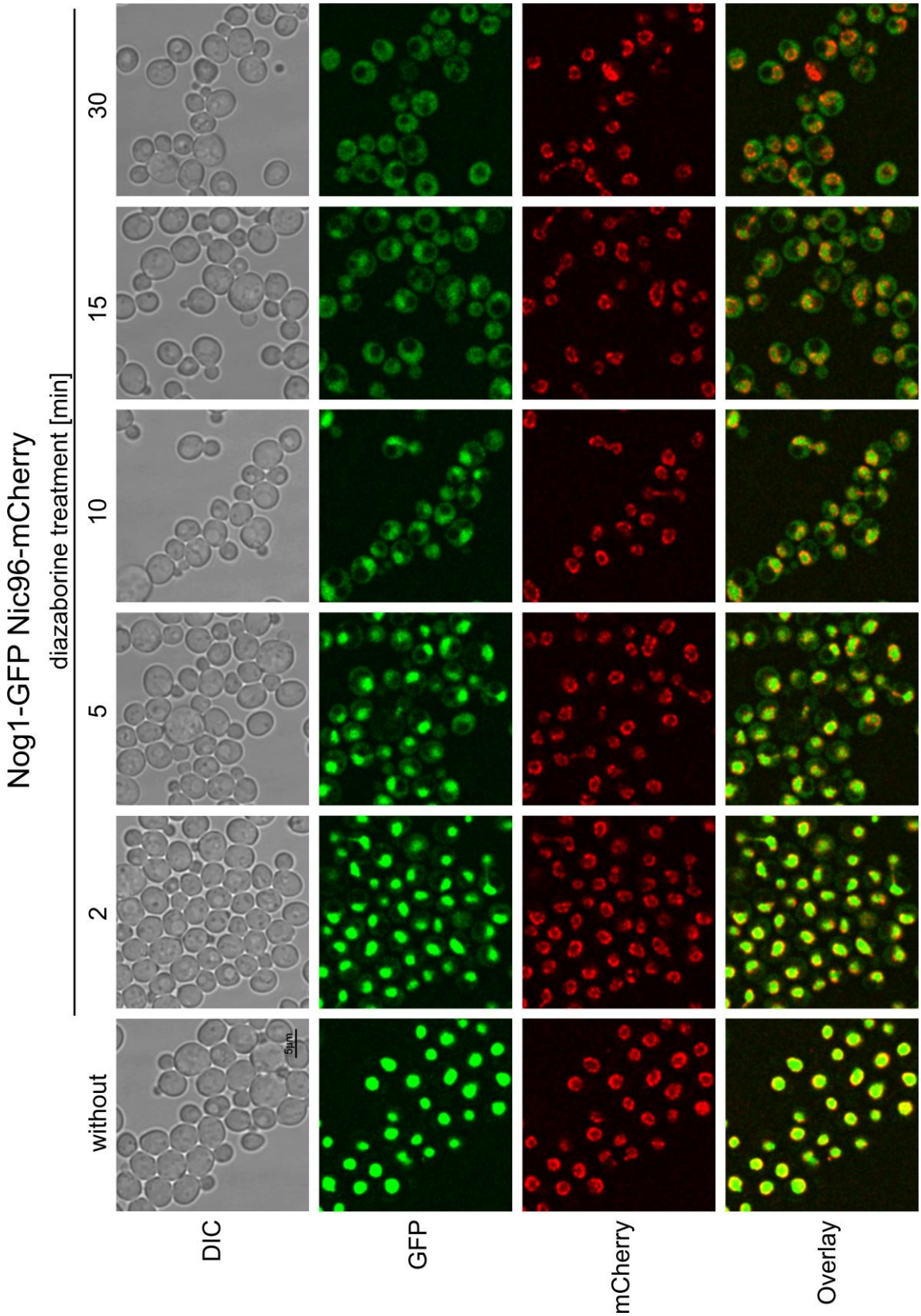

Figure 9: Nog1 exhibits complete nuclear depletion after 30 minutes of diazaborine treatment. Cells were grown and treated according to the standard procedure depicted in 2.11.2.1. Nic96 served as nuclear marker protein. Nog1 showed an initial localization in the nucleus and started to accumulate in the cytoplasm after 2 minutes. After 30 minutes a complete nuclear depletion occurred.

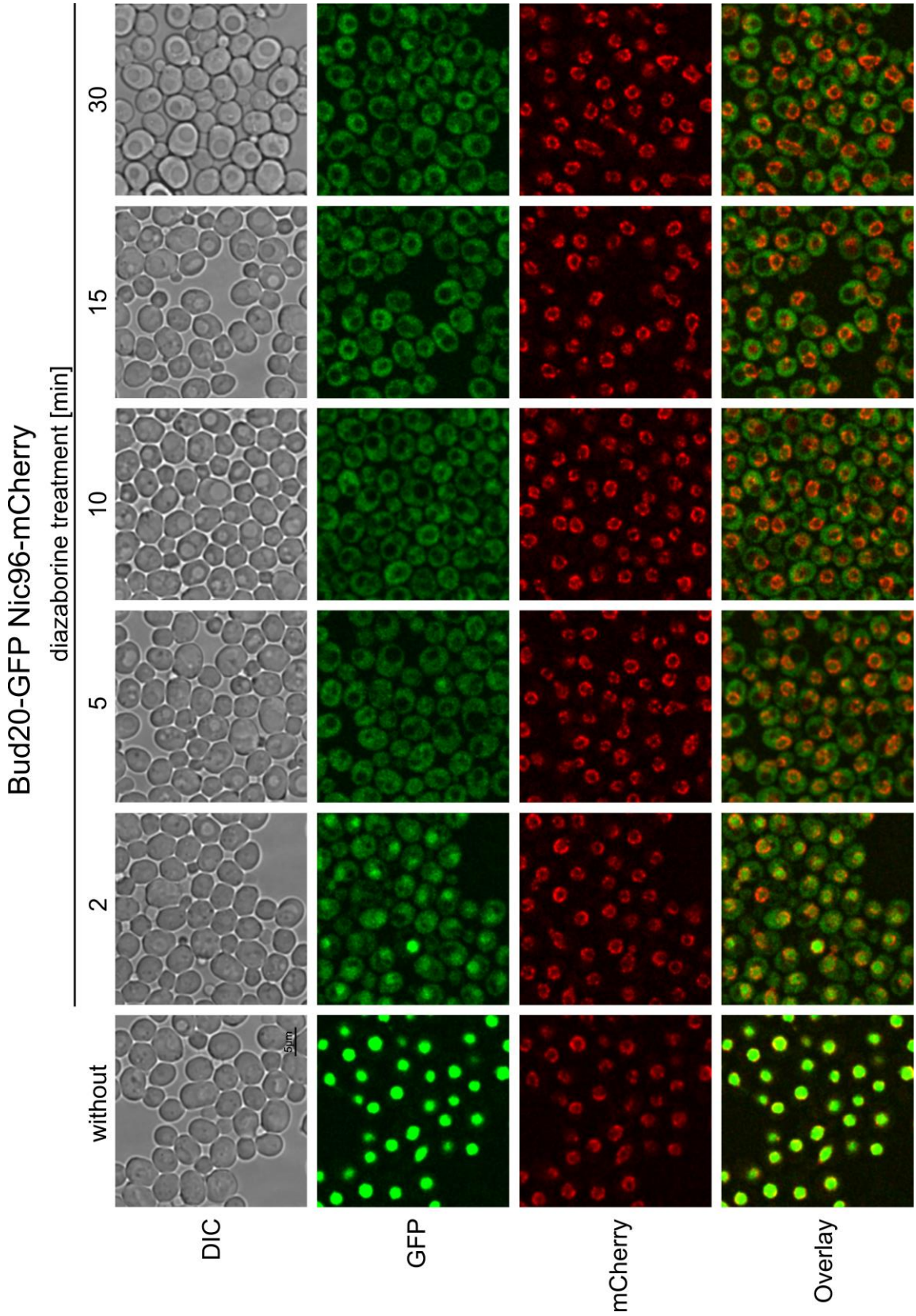

Figure 10: Bud20 exhibits a complete nuclear depletion after 5 minutes of diazaborine treatment. Cells were grown and treated according to the standard procedure depicted in 2.11.2.1. Nic96 served as nuclear marker protein. Bud20 showed an initial localization in the nucleus and started to accumulate in the cytoplasm after 2 minutes of diazaborine treatment. After 10 minutes of treatment a complete nuclear depletion occurred.

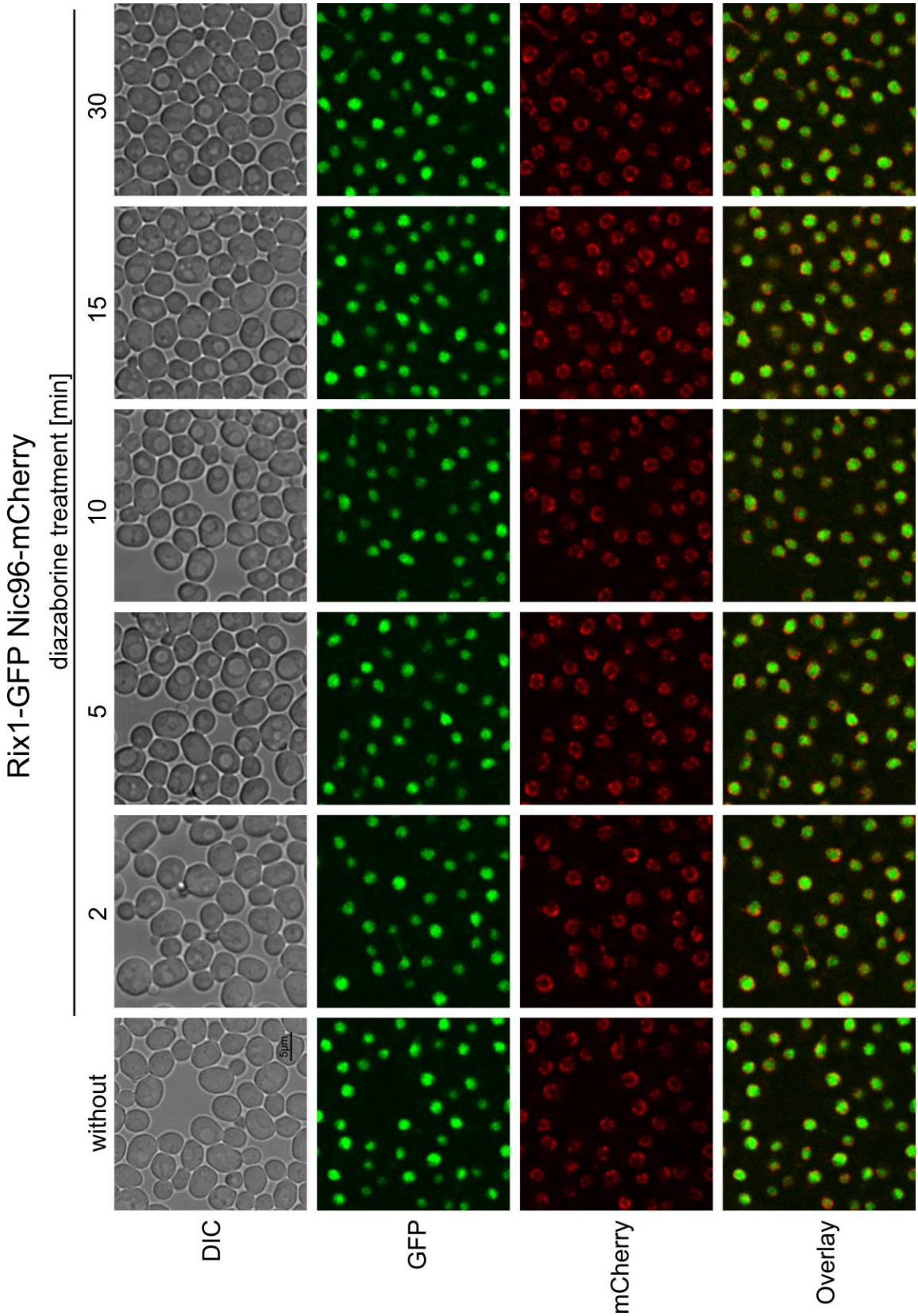

Figure 11: The nucleoplasmic maturation factor Rix1 does not alter its localization upon diazaborine treatment. Cells were grown and treated according to the standard procedure depicted in 2.11.2.1. Nic96 served as nuclear marker protein. Rix1 showed a nucleoplasmic localization during the whole period of treatment.

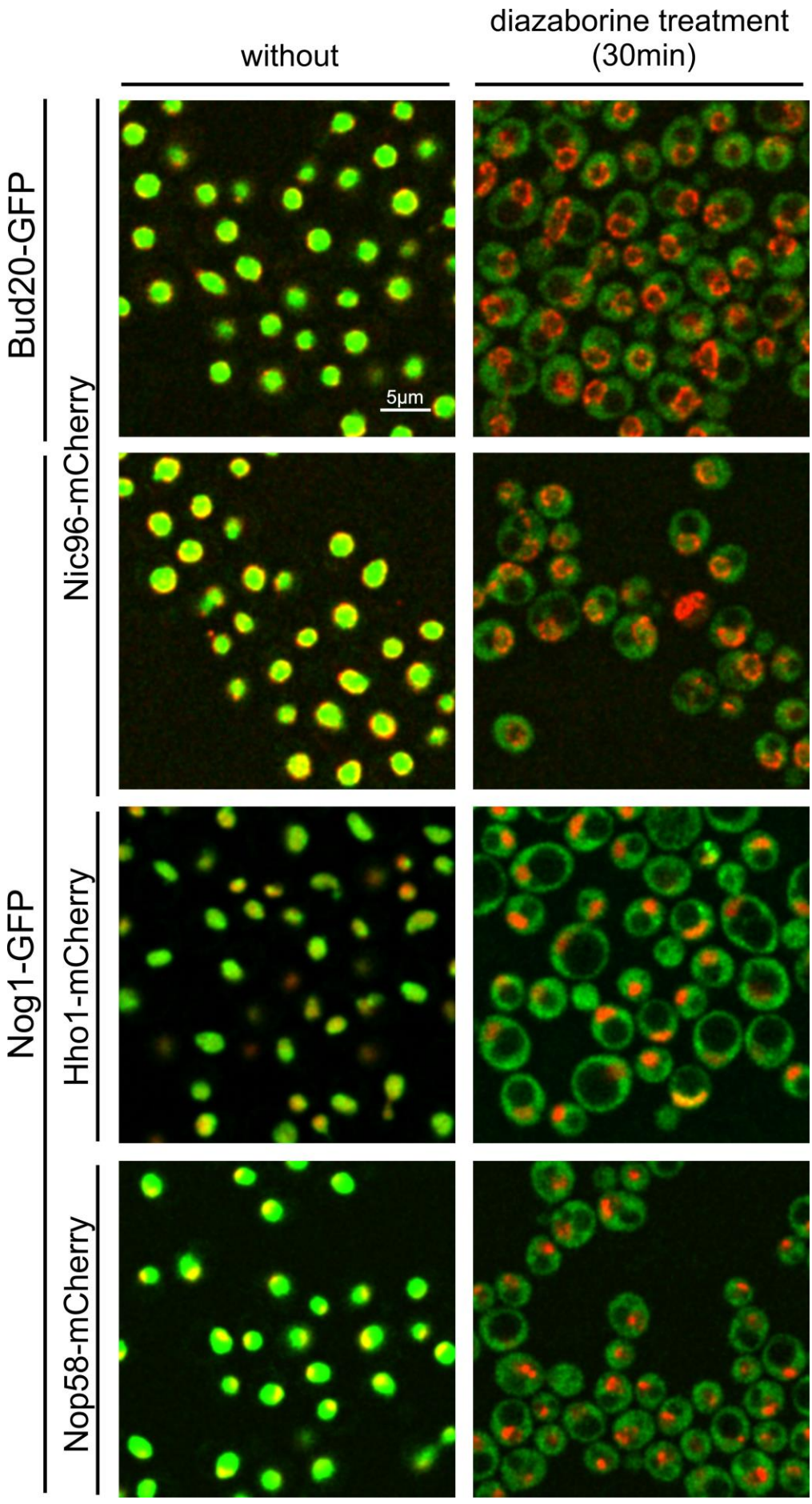
without
diazaborine treatment
(30min)
Bud20-GFP
Nic96-mCherry
Nog1-GFP
Hho1-mCherry
Nop58-mCherry
5μm

Figure 12 Enlarged view of the shuttling factors Bud20-GFP and Nog1-GFP in the absence and presence of diazaborine. Cells were grown and treated according to the standard procedure depicted in 2.11.2.1. Bud20-GFP as well as Nog1-GFP showed a nuclear and nucleolar depletion, respectively after 30 minutes of diazaborine treatment. Colocalization was tested with the indicated mCherry fusions.

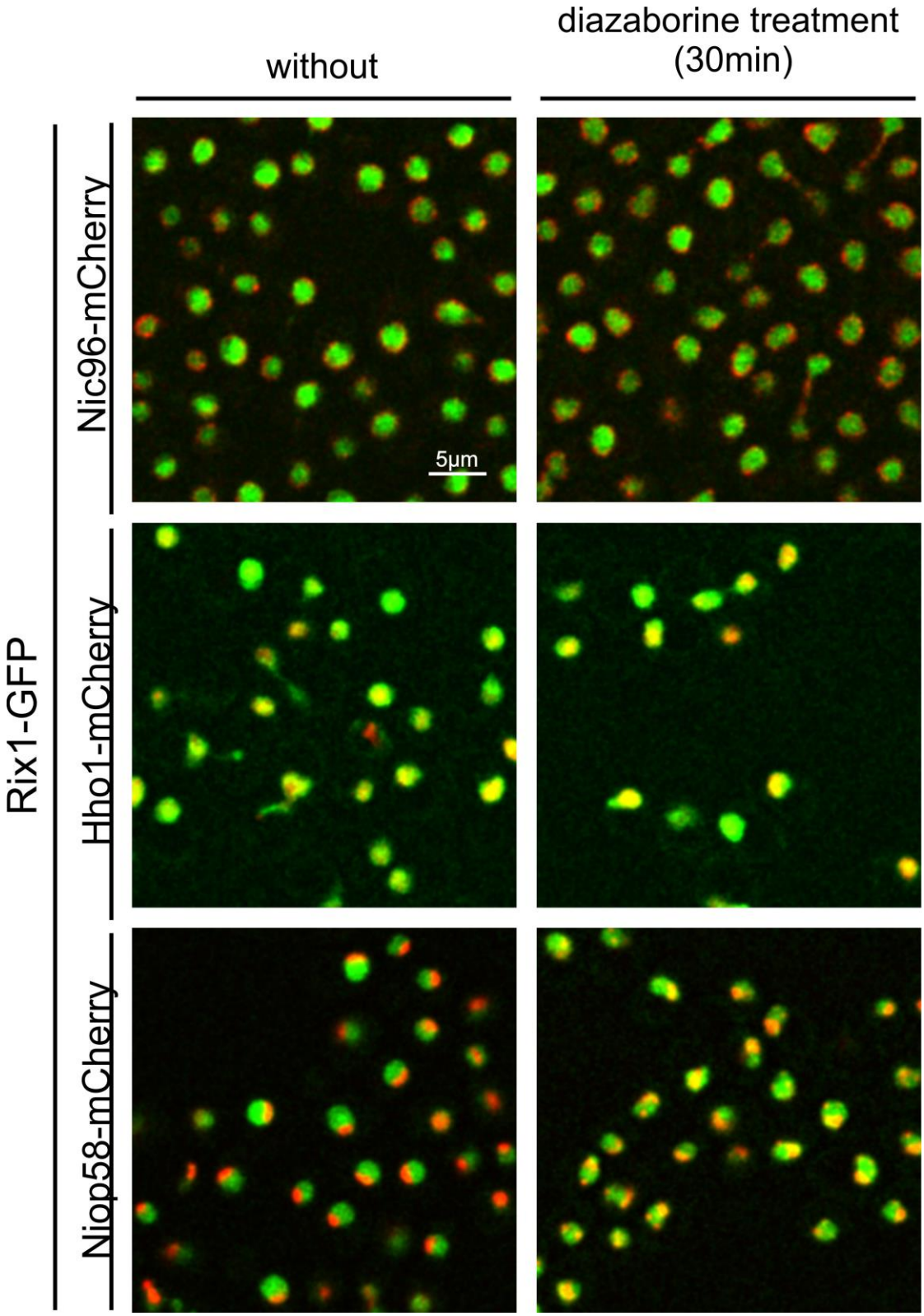

Figure 13: Enlarged view of Rix1-GFP in the absence and presence of diazaborine. Cells were grown and treated according to the standard procedure depicted in 2.11.2.1. Rix1 showed a strict nucleoplasmic localization after 30 minutes of diazaborine treatment. Colocalization was tested with the indicated mCherry fusions

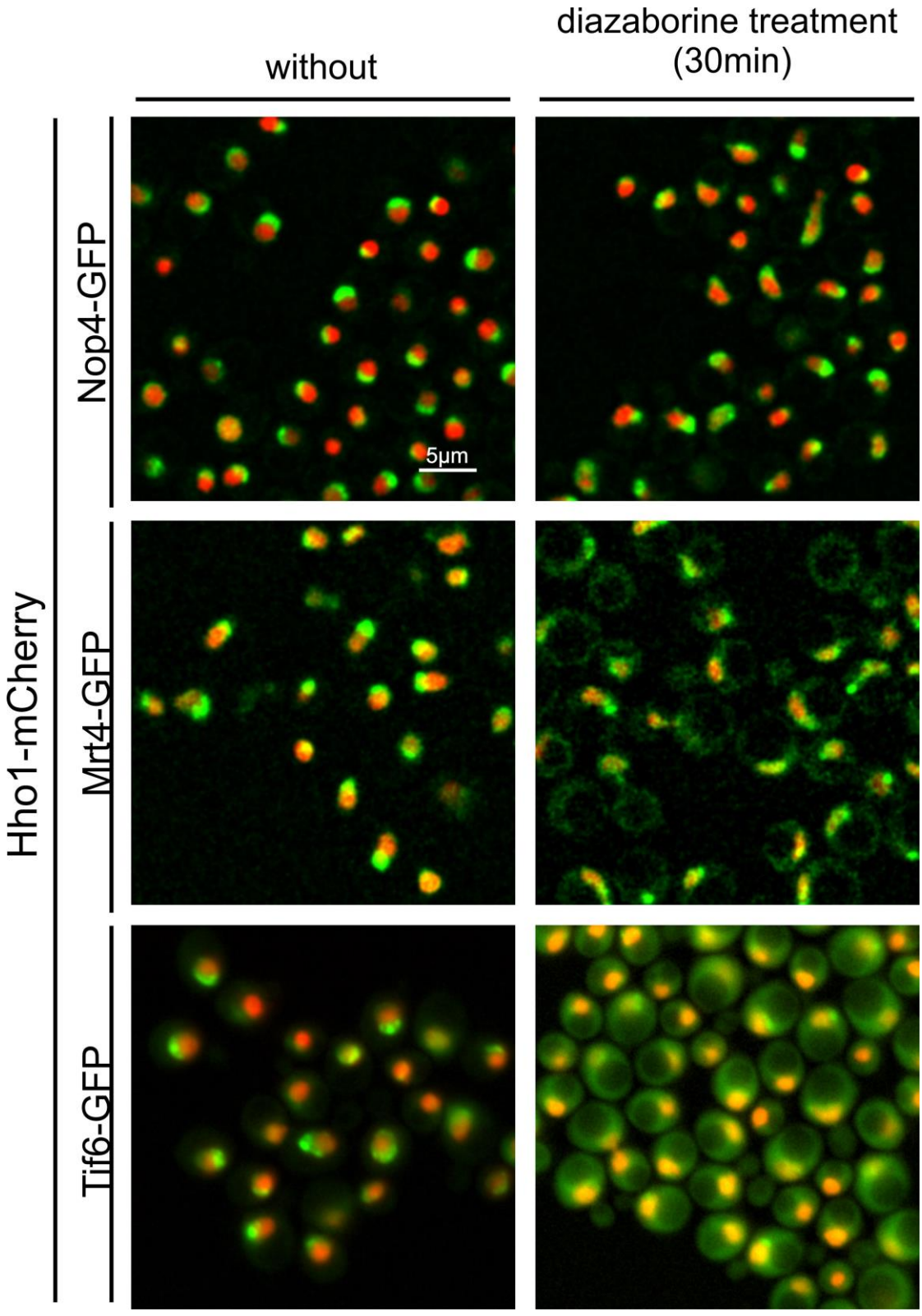

Figure 14: Enlarged view of Nop4-, Mrt4- and Tif6-GFP in the absence and presence of the inhibitor diazaborine. Cells were grown and treated according to the standard procedure depicted in 2.11.2.1. Tif6 pictures were taken by the use of the Axioskop Fluorescence microscope, while the other pictures were taken using a laser scanning microscope. Initially Nop4 showed mainly a nucleolar localization, in contrast to Mrt4 and Tif6 which showed a mainly nucleolar and a nucleoplasmic localization. After 30 minutes of diazaborine treatment Nop4 showed a stronger nucleoplasmic and even cytoplasmic signal including tiny nucleoplasmic accumulation dots. Mrt4 and Tif6 should a cytoplasmic accumulation including a remaining nuclear signal after 30 minutes of diazaborine treatment.

Without diazaborine treatment 88% of the whole fluorescence signal of Bud20-GFP and 82% of Nog1-GFP, respectively was located in the nucleus. In contrast to Nog1, Bud20 rapidly accumulated in the cytoplasm. Already after 2 minutes of diazaborine treatment only 35% of the fluorescence signal of Bud20 was detected in the nucleus. After 10 minutes of treatment the signal in the nucleus diminished to 22% and stayed constant until the remaining period of drug treatment. Nog1 entered the cytoplasm significantly slower than Bud20. After 2 minutes still 77% of the fluorescence signal remained in the nucleus. After 10 minutes 47% of the whole signal remained in the nucleus but after 30 minutes of drug treatment the remaining fluorescence signal in the nucleus corresponded to that of Bud20. In contrast, Rix1 showed over the whole period of treatment a fluorescence signal of approximately 92% in the nucleus (Figure 15). Since Bud20 accumulated much faster in the cytoplasm than Nog1 the nucleus was earlier depleted of Bud20. This could be seen on the overlay where the nuclear signal was clearly red (Figure 9, Figure 10, Figure 11). An enlarged version of the microscopy pictures of Bud20, Nog1 and Rix1 without and upon 30 minutes of diazaborine treatment is shown in Figure 12 and Figure 13.

Considering the Nog1-GFP Hho1-mCherry experiment it was obvious that Nog1 locates in the nucleolus as well as in the nucleoplasm. After diazaborine treatment it left the nucleolus and located in the nucleoplasm during its way to the cytoplasm (Figure 4). To be able to investigate the exact alteration of the nucle(ol)ar localization of Nog1 upon diazaborine treatment and also to include the temporal aspects, the nucleolar maturation factor Nop58 was tagged with mCherry and colocalization studies with Nog1 were performed.
Investigation of the depletion of the nucleolus by Nog1 revealed a fluorescence signal in the nucleolus without diazaborine treatment of 21%. The signal diminished to 16% and 8% upon treatment with diazaborine for 2 and 5 minutes, respectively. After 10 minutes of treatment 7% of the whole fluorescence signal remained in the nucleolus. The time Nog1 needed to leave the nucleolus corresponded approximately to the time it needed to leave the whole nucleus (Figure 15). After 10 minutes of treatment it was not possible any more to quantify the amount of the fluorescence signal of Nog1 regarding its localization in the nucleolus due to an occurring fragmentation of the nucleolar factor Nop58 upon diazaborine treatment (Figure 16).
In addition to the quantification of temporal aspects of diazaborine inhibition the concentration of GFP molecules in the nucle(ol)us should be quantified. Therefore a standard curve with purified GFP was prepared and measured in presence or absence of diazaborine (Figure 17). Adjacently cells were mixed with specific standard concentrations and investigated by fluorescence microscopy. The intensity of the nucleus/nucleolus of 100

cells was determined and the mean value was used to calculate the concentration of GFP molecules (Figure 20).

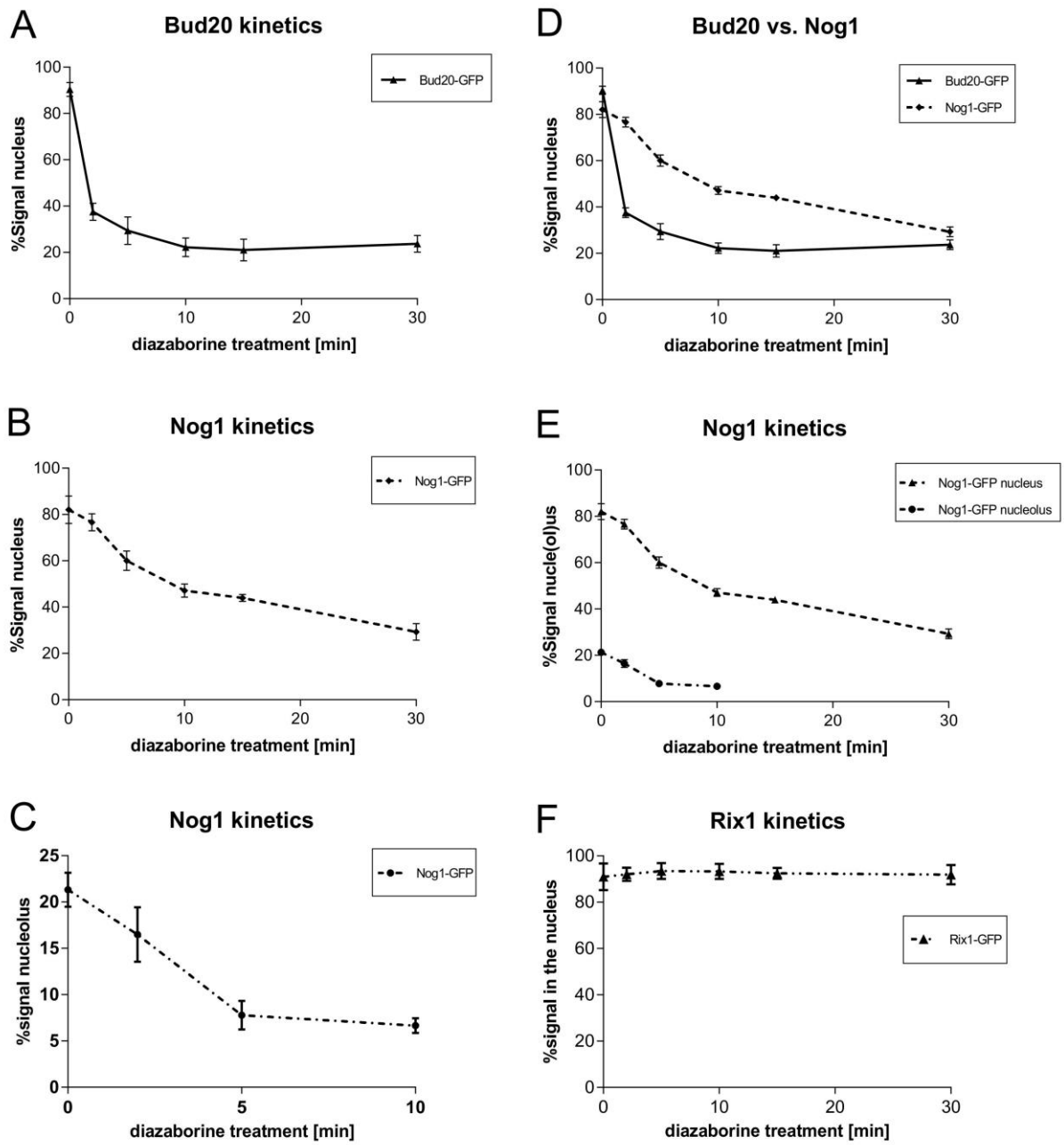

Figure 15: Kinetic analysis of the localization of shuttling factors Nog1 and Bud20 and the nucleoplasmic factor Rix1 upon treatment with 10µg/ml diazaborine. The analysis was performed by evaluation of fluorescence intensities derived by fluorescence microscopy. Prior to microscopy cells exhibiting an OD_{600} of 0.4-0.5 were treated with 10µg/ml diazaborine for the indicated periods of time. Nic96 and Nop58 served as marker for the nucleus and the nucleolus, respectively. Bud20 showed roughly a total depletion of the detected fluorescence signal in the nucleus already after 2 minutes of diazaborine treatment (37% fluorescence signal) whereas Nog1 required 30 minutes of treatment for the same extent of nuclear depletion. Without treatment 21% of Nog1-GFP fluorescence signal located in the nucleolus. After treatment with diazaborine for 10 minutes only 7% of Nog1s fluorescence signal was detectable in the nucleolus. After 10 minutes the investigation had to be stopped due to an occurring nucleolar fragmentation. **(A)** Kinetics of Bud20 containing particles upon diazaborine treatment regarding the nucleus marked by Nic96-mCherry. **(B)** Kinetics of Nog1 containing particles regarding the nucleus flanked by Nic96-mCherry. **(C)** Kinetics of Nog1 containing particles regarding the nucleolus marked by Nop58-mCherry. **(D)** Comparison between the kinetics of Bud20 and Nog1 regarding the nucleus. **(E)** Comparison of the kinetics of Nog1 between the nucleus and the nucleolus. **(F)** Kinetics of Rix1 containing particles regarding the nucleus marked by Nic96-mCherry

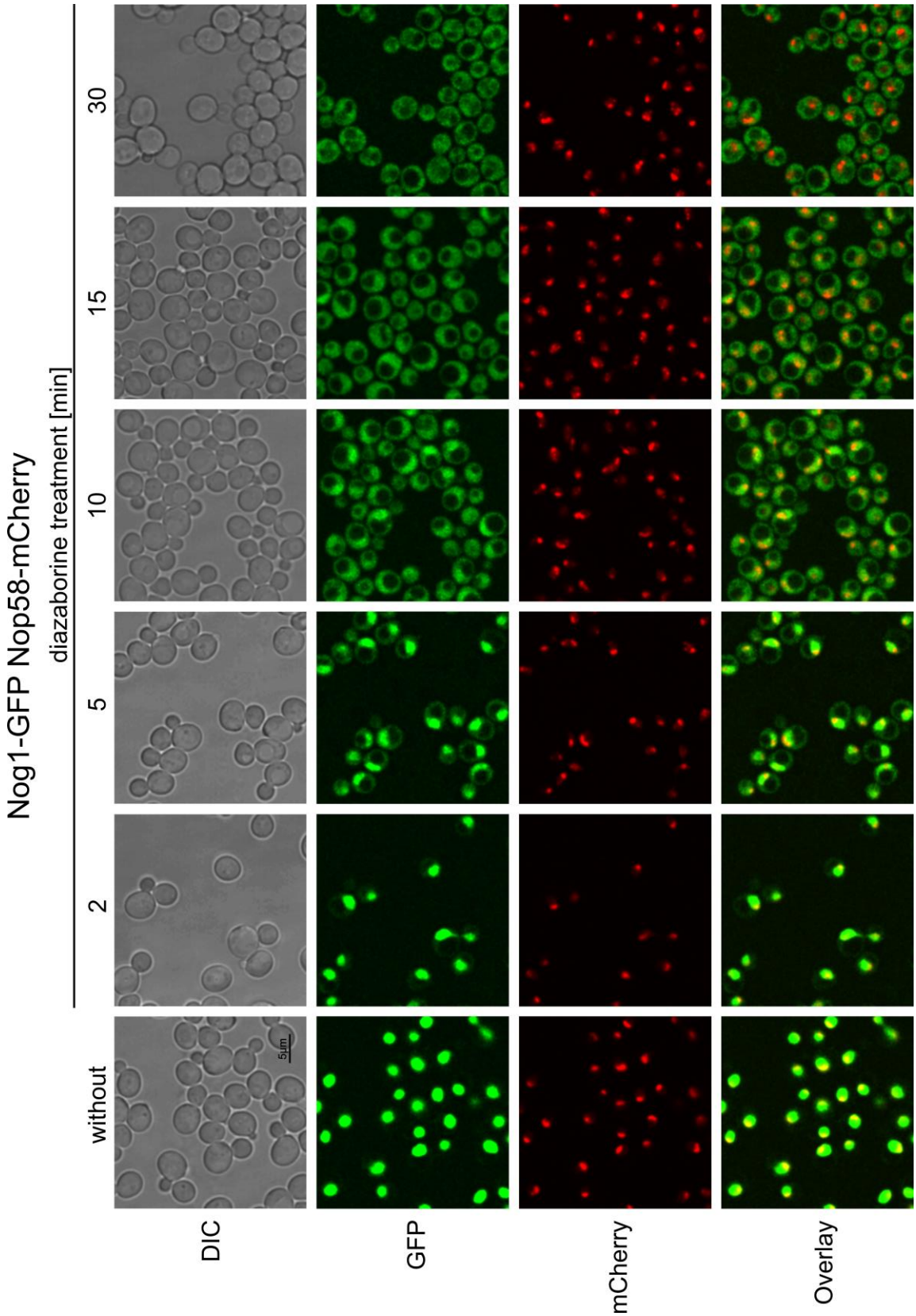

Figure 16: The shuttling factor Nog1 exhibits nucleolar depletion after 10 minutes of diazaborine treatment. Cells were grown and treated according to the standard procedure depicted in 2.11.2.1. Nog1 showed an initial localization in the nucleolus and nucleoplasm, started to leave the nucleus after 2 minutes and showed a complete depletion of the nucleus after 30 minutes. Nog1 left mainly the nucleolus after 10 minutes of diazaborine treatment. The nucleolar factor Nop58 showed a beginning fragmentation after 10 minutes of diazaborine treatment.

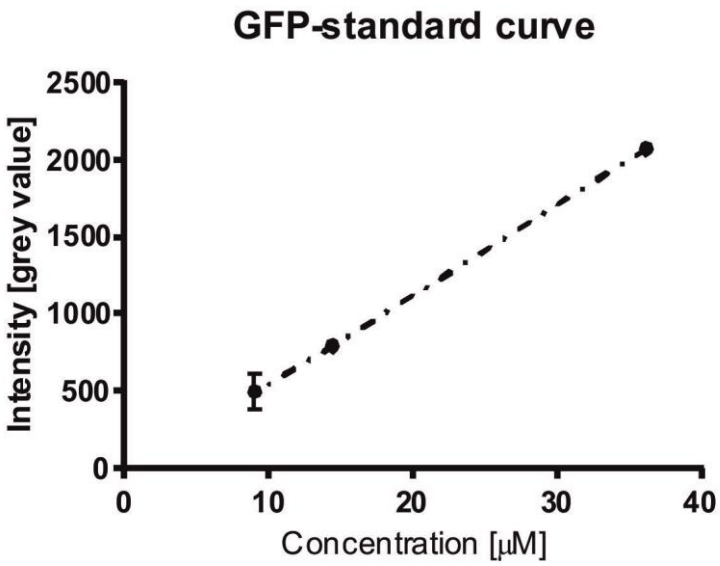

Figure 17: GFP-standard curve used for the quantification of GFP concentrations in the strains Nog1-GFP and Bud20-GFP. The purified GFP was solved in buffer A (see Table 12). Mean value and standard deviation were calculated from 3 biological replicates.

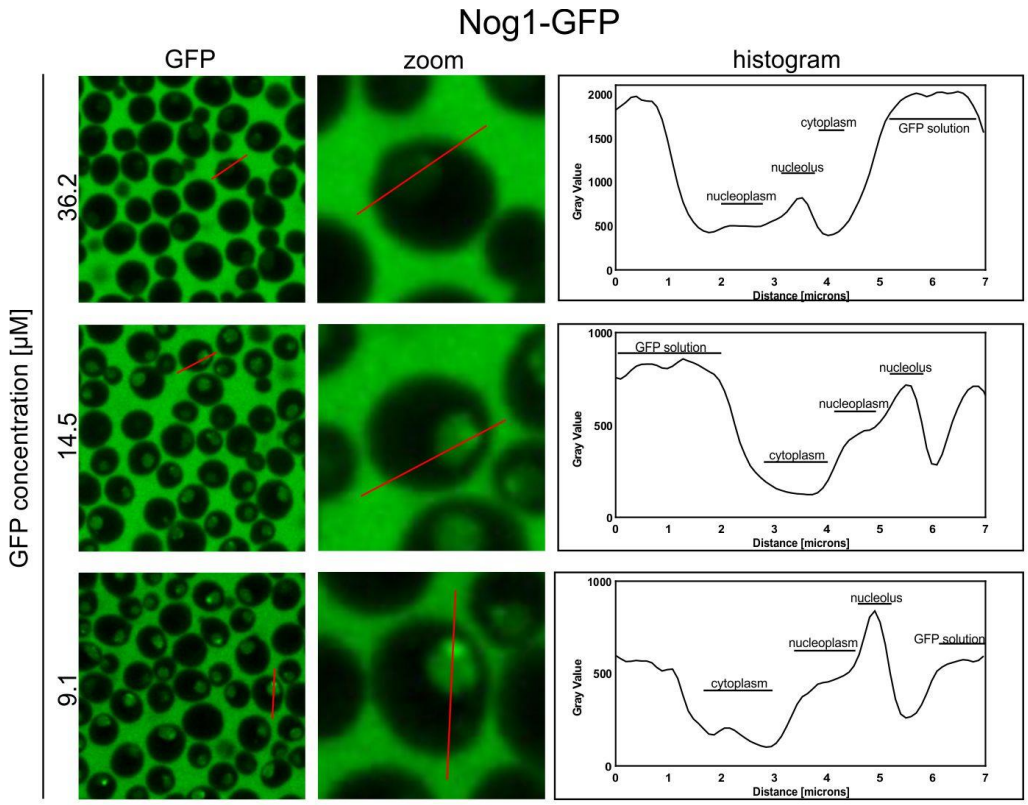

Figure 18: Determination of nucle(ol)ar Nog1-GFP concentrations using GFP solutions with indicated concentrations. Intensity plots of cross sections (red lines) of exemplary cells are shown on the left. The intensity plots revealed 14.5µM as approximate GFP concentration in the nucleolus and 9.1µM in the nucleoplasm of Nog1.

Pictures of cells mixed with GFP solutions of known concentrations and the corresponding linear intensity plot of the marked cross sections are shown in Figure 18 and Figure 19. The nucleoli of Nog1 showed an intensity of approximately 750 gray value intensities and the nucleoplasm approximately 500 gray value intensities at all three GFP concentrations. On the histogram regarding 36.2µM GFP the surrounding GFP concentration was much higher than the nuleolar and nucleoplasmic concentration. On the histogram of 14.5µM GFP the intensity of the nucleolus corresponded approximately to the intensity of the surrounding GFP solution whereas the histogram of 9.1µM showed lower intensities of the GFP solution compared to the nucleolus of the cells. Moreover the intensities of 14.5µM and 9.1µM GFP were higher than the GFP signal in the nucleoplasm, concluding an approximate GFP concentration of 14.5µM in the nucleolus and a concentration below 9.1µM in the nucleoplasm for Nog1 (Figure 18). Considering Bud20 the GFP solution exhibiting a concentration of 14.5µM showed a higher intensity than the nuclear signal whereas the intensity of the GFP solution exhibiting a concentration of 9.1µM corresponded to the intensity of the nucleus of Bud20. This leads to the conclusion that Bud20-GFP exhibits a concentration of 9.1µM in the nucleus (Figure 19).

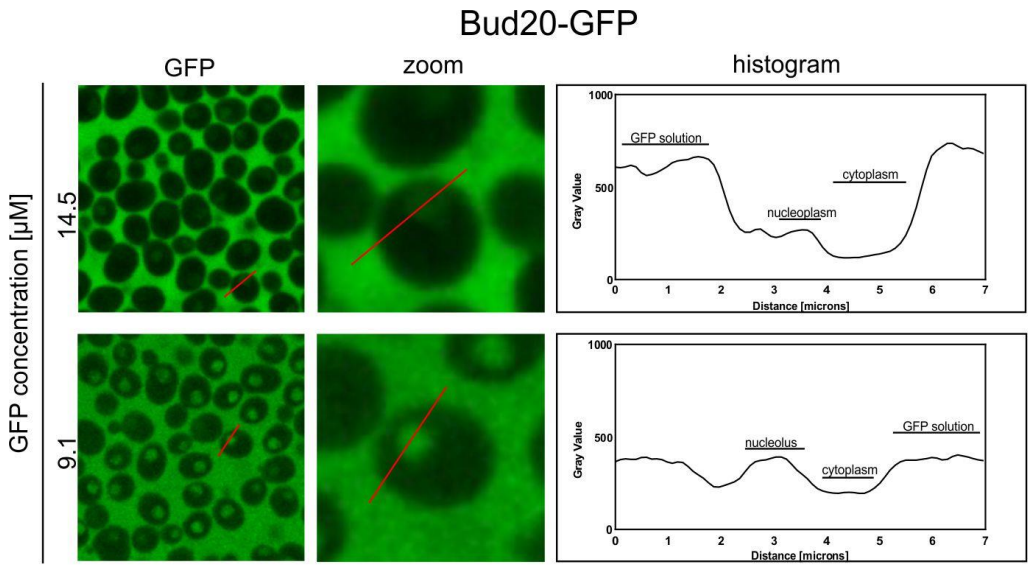

Figure 19: Determination of nuclear Bud20-GFP concentrations using GFP solutions with indicated concentrations. Intensity plots of cross sections (red lines) of exemplary cells are shown on the right. The intensity plots revealed a nuclear GFP concentration of Bud20-GFP approximately 9.1µM.

The exact calculation of the GFP concentrations in the nucle(ol)us of Nog1 and Bud20 using the previously generated standard curve revealed 11.8µM ± 2.2µM GFP in the nucleolus, 7.7µM ± 0.9µM in the nucleoplasm of Nog1 and 4.0µM ± 0.2µM in the nucleus of Bud20 (Figure 21).

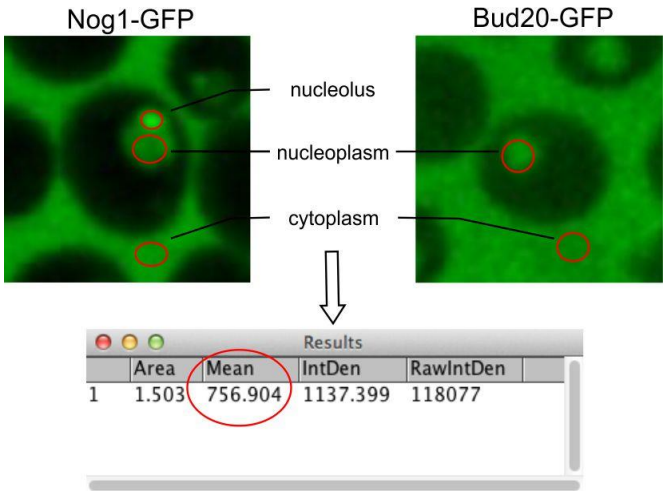

Figure 20: GFP quantification procedure of Nog1-GFP and Bud20-GFP. The mean intensity of the indicated areas was measured of 100 cells and a mean value and standard deviation was calculated.

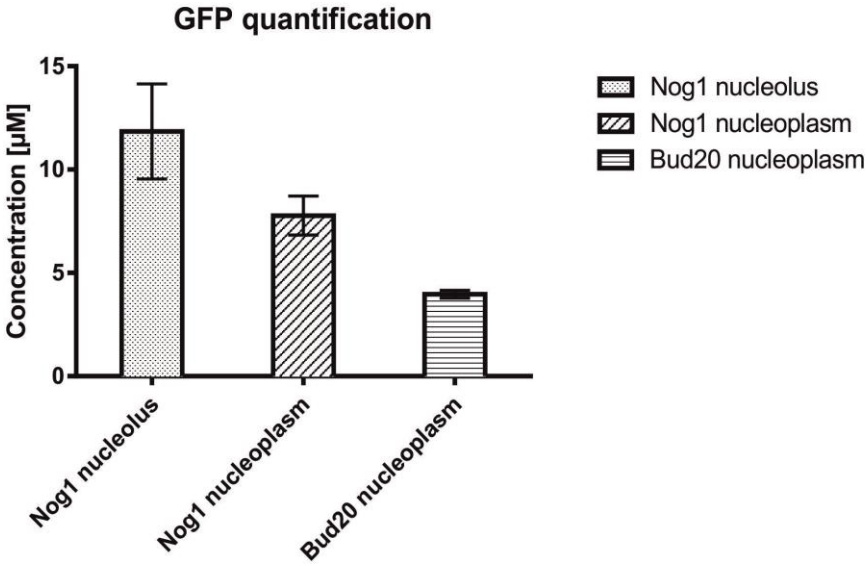

Figure 21: Quantification of Nog1-GFP and Bud20-GFP concentrations present in the nucle(ol)us or the nucleoplasm. For the quantification a standard curve (see **Figure 17**) was used. The quantification revealed 11.8µM ± 2.2µM GFP in the nucleolus, 7.7µM ± 0.9µM in the nucleoplasm of Nog1 and 4.0µM ± 0.2µM GFP in the nucleus of Bud20.

3.1.1.4 Impact of diazaborine on early steps of the pre-60S maturation

For further investigation of the nucleolar fragmentation upon diazaborine inhibition GFP tagged versions of Noc2 and the nucleolar to nucleoplasmic factor Nsa1 were examined. Additionally Nop58 was mCherry tagged and the colocalization was investigated before and after diazaborine treatment, respectively.

Consistent with literature Noc2-GFP showed a nucleolar localization in the absence of diazaborine. After 30 minutes of treatment with diazaborine Noc2-GFP covered an enlarged area and showed tiny accumulation spots corresponding to the fragmentation pattern of

Nop58 (Figure 22). Nsa1 showed a nucleolar and a weak nucleoplasmic localization without diazaborine treatment. After 30 minutes of treatment the covered area seemed to expand similar to Noc2. Indeed, the tiny accumulation spots occurred to a lesser extent than for Noc2 and they did not show a high degree of colocalization with Nop58 (Figure 22).

As shown before Noc2 and Nsa1 altered their localization upon diazaborine treatment including the formation of small, strongly fluorescing spots. To test, whether these spots are localized in the nucleoplasm the *HHO1* of Noc2-GFP and Nsa1-GFP expressing strains were also tagged with mCherry to mark the nucleoplasm.

Without diazaborine treatment the factor Noc2 located strictly in the nucleolus as shown before. Nsa1-GFP showed a nucleolar and nucleoplasmic localization without treatment. After treatment with diazaborine the tiny spots of Noc2-GFP seemed to localize in the nucleoplasm because of the significant colocaliziation with the nucleoplasmic marker Hho1. In contrast to Noc2 the occurring accumulation spots of Nsa1 did not seem to localize in the nucleoplasm (Figure 23).

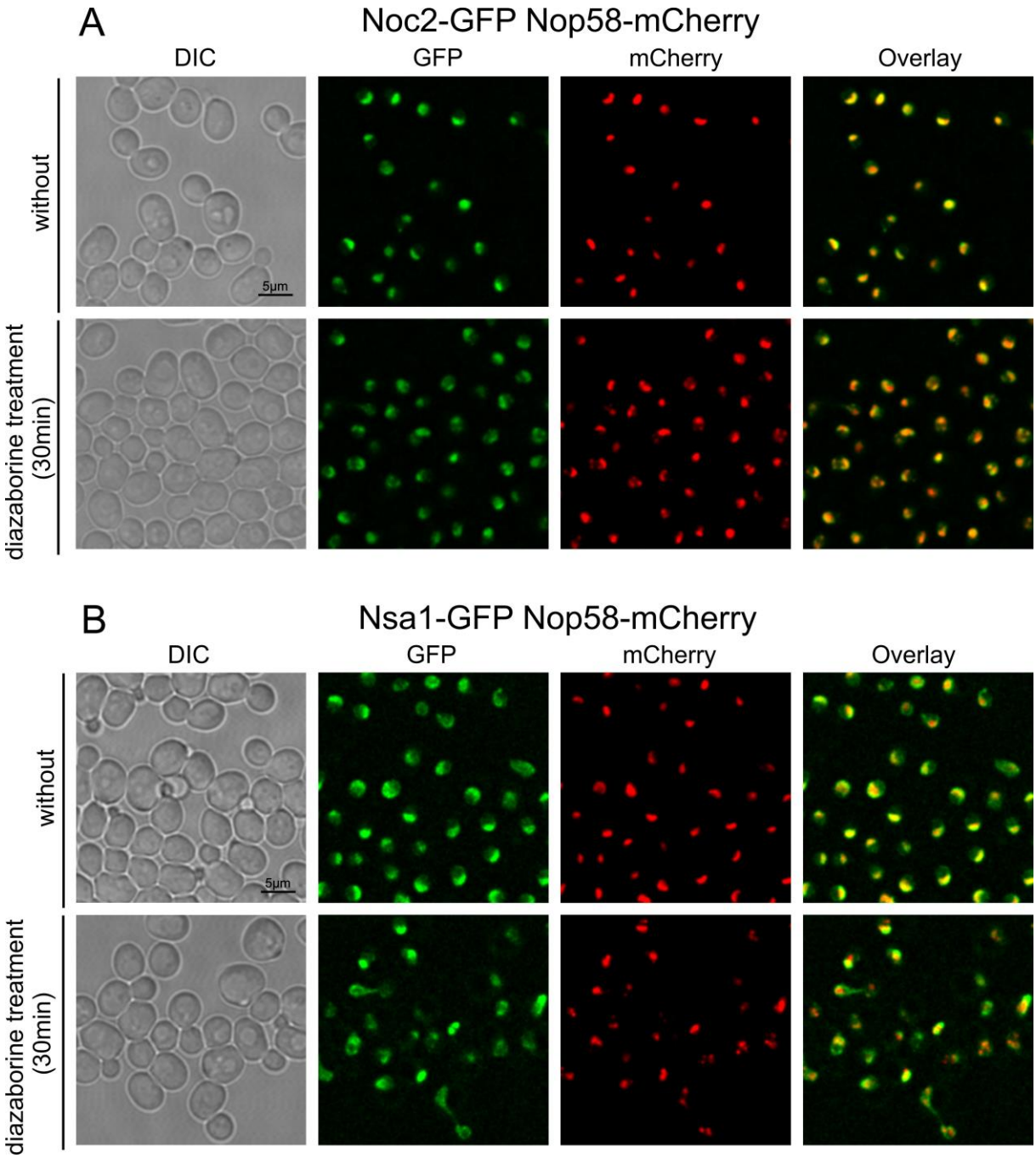

Figure 22: Colocalization studies of Noc2 or Nsa1 with nucleolar Nop58-mCherry after diazaborine treatment. Cells were grown and treated according to the standard procedure depicted in 2.11.2.1. **(A)** Noc2 showed a steady-state localization in the nucleolus and started to accumulate in tiny spots after treatment with diazaborine. Also Nop58 located initially in the nucleolus and accumulated in tiny spots. Noc2 and Nop58 showed a high degree of colocalization with as well as without diazaborine. **(B)** Nsa1 showed a steady-state localization in the nucleoplasm and the nucleolus and started to accumulate in tiny spots after treatment with diazaborine. Also Nop58 located initially in the nucleolus and accumulated in tiny spots. Indeed, Nsa1 and Nop58 showed a low degree of colocalization in the presence of diazaborine.

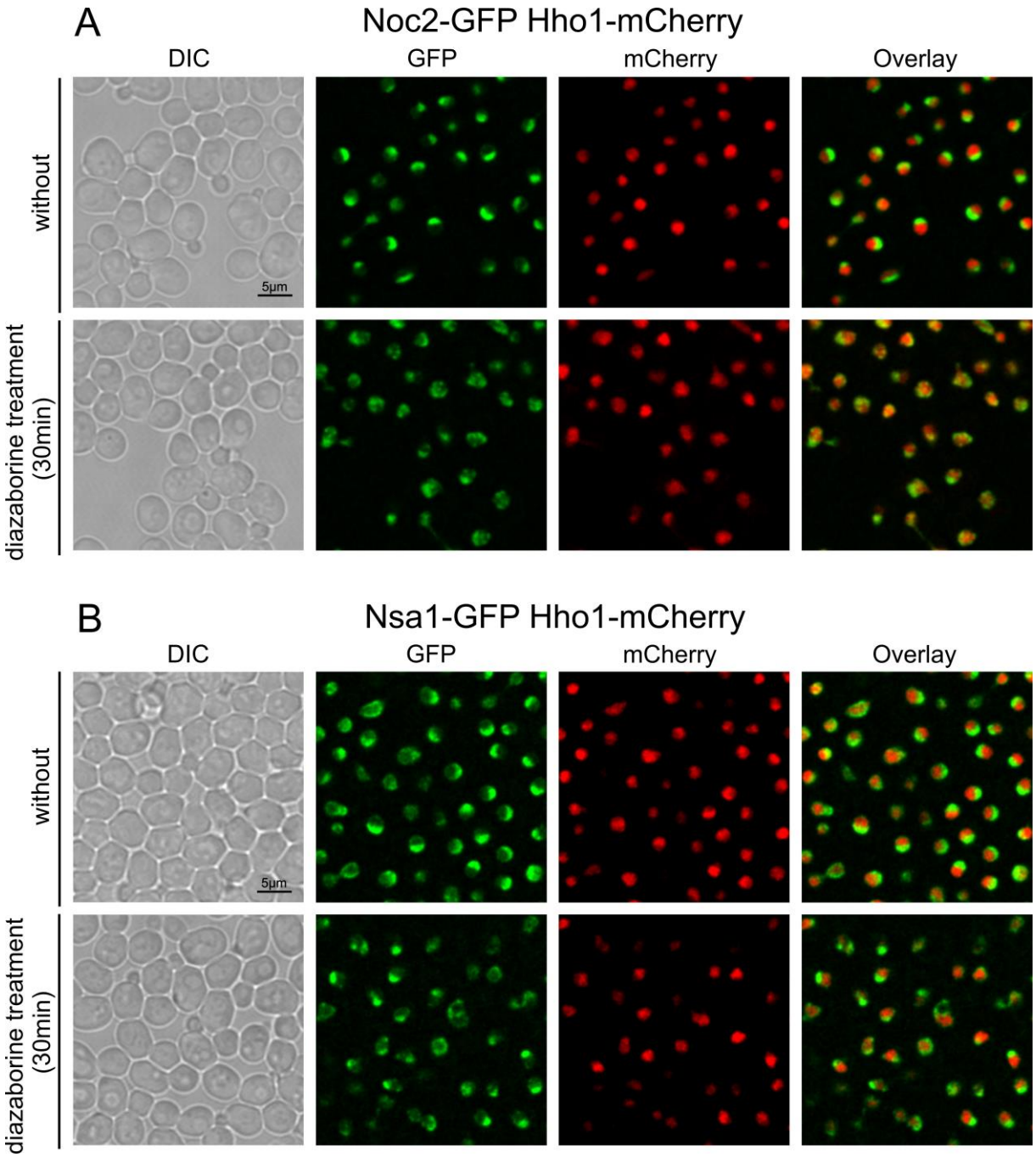

Figure 23: Colocalization studies of Noc2 or Nsa1 with nucleoplasmic Hho1-mCherry upon diazaborine treatment. Cells were grown and treated according to the standard procedure depicted in 2.11.2.1. The nucleoplasmic marker Hho1 did not alter its localization during the whole period of diazaborine treatment **(A)** Initially Noc2 showed a nucleolar localization without treatment. After treatment with diazaborine tiny accumulation spots occurred and showed colocalization with Hho1-mCherry to a very high extent. **(B)** Nsa1 showed a nucleolar to slight nucleoplasmic localization without diazaborine treatment. After treatment small spots formed but did not show a high degree of colocalization with Hho1.

Since Rix1 exhibited a strict nucleoplasmic localization even after diazaborine treatment (Figure 5), it was used to investigate the localization of the spots occurring of Nop58 upon diazaborine treatment. Therefore cells were grown to an OD_{600} of 0.4-0.5 prior to the addition of 10µg/ml diazaborine in liquid culture to subsequent application on agar coated slides supplied with all amino acids and 100µg/ml diazaborine.

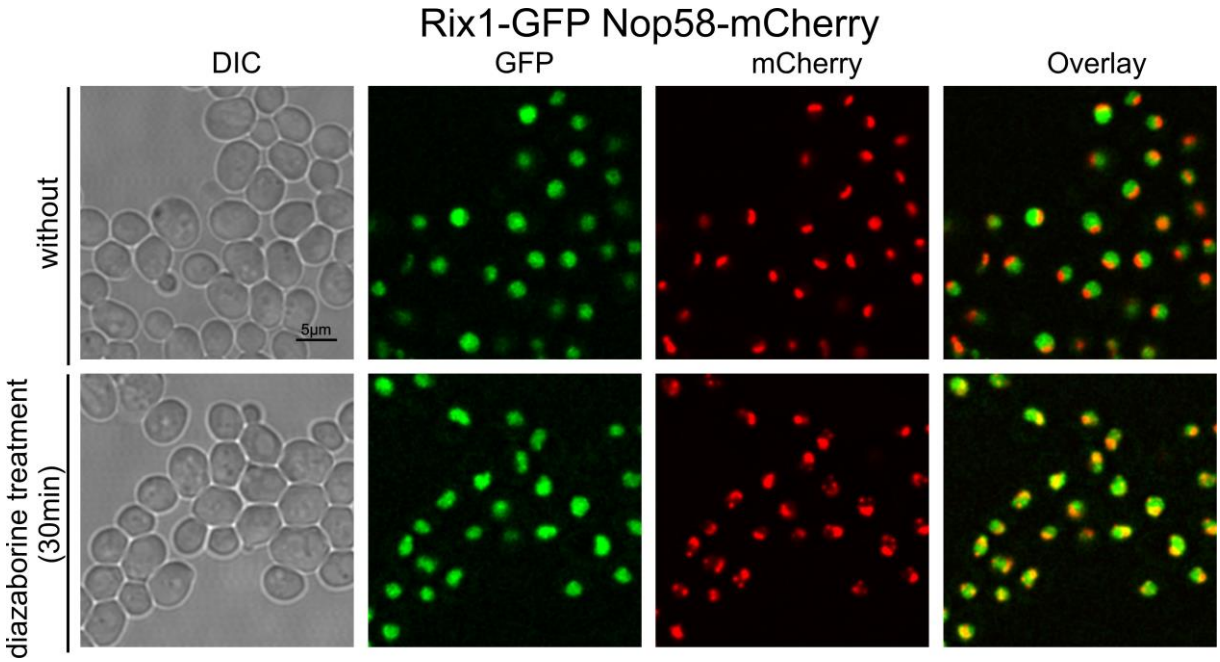

Figure 24: The nucleolar factor Nop58 exhibits nucleoplasmic spots upon diazaborine treatment. Cells were grown and treated according to the standard procedure depicted in 2.11.2.1. The nucleoplasmic factor Rix1 served as nucleoplasmic marker. Without diazaborine treatment Nop58 showed nucleolar localization. After treatment with diazaborine small accumulation spots were formed showing colocalization with Rix1 to a high extent.

Nop58 showed a nucleolar steady-state localization without diazaborine treatment as already shown before. After treatment small spots occurred exhibiting a high degree of colocalization with Rix1 (Figure 24). This experiment further confirmed the assumption that the accumulating spots observed for the nucleolar factor Nop58, as well as for Noc2, were localized in the nucleoplasm after diazaborine treatment. An enlarged version of the microscopy pictures of Rix1 in the absence and presence of diazaborine for 30 minutes is shown in Figure 13.

The nucleolar factor Nop4 was known to interact with Nop1 being part of Nop58- containing particles (Lafontaine & Tollervey 1999). Additionally the factor showed a similar fragmentation pattern upon diazaborine treatment as derived for Nop58 (Pertschy et al. 2004). Thus, the set-up should be further tested by the investigation of the effect of diazaborine on the nucleolar factor Nop4. For investigation of a possible nucleoplasmic accumulation, the histone H1 (Hho1) served as nucleoplasmic marker. Therefore cells were grown to an OD_{600} of 0.4-0.5 prior to the addition of 10µg/ml diazaborine into the liquid

culture to subsequent application on agar coated slides supplied with all amino acids and 100µg/ml diazaborine.

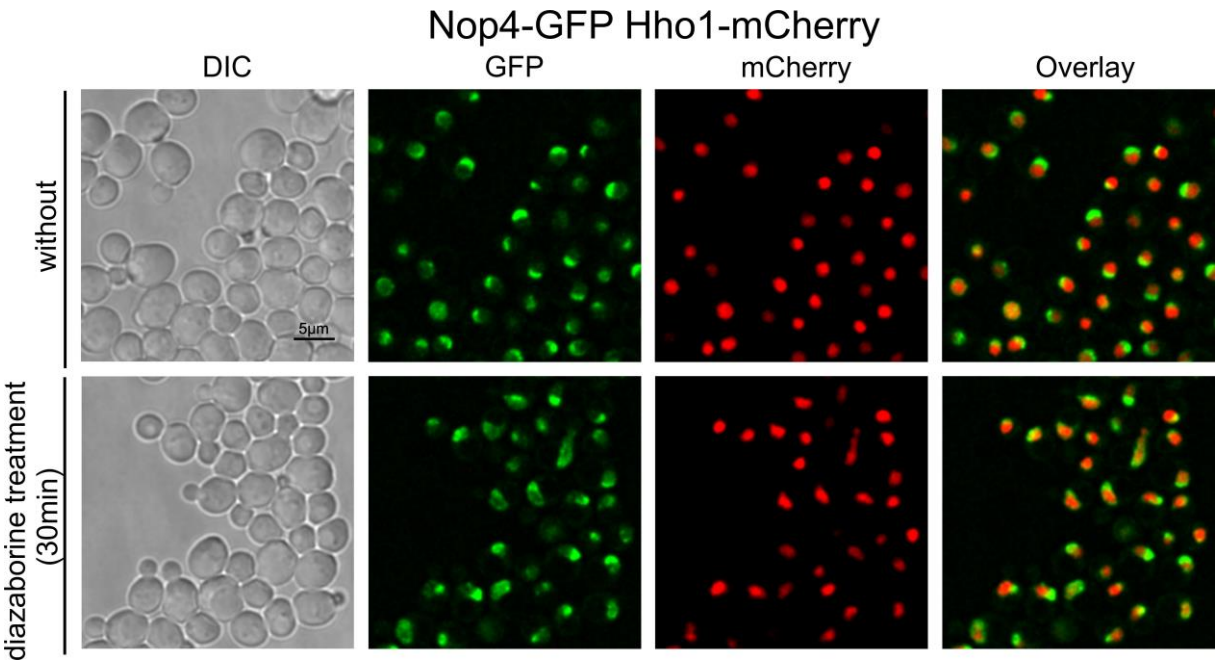

Figure 25: Nop4-GFP shifts towards the nucleoplasm and accumulates in spots upon diazaborine treatment. Cells were grown and treated according to the standard procedure depicted in 2.11.2.1. Nop4 showed an initial nucleolar to slight nucleoplasmic localization. After 30 minutes of diazaborine treatment Nop4 showed a stronger nucleoplasmic and even cytoplasmic signal including tiny nucleoplasmic accumulation dots.

The nucleolar factor Nop4 showed an initial nucleolar to slight nucleoplasmic localization. After 30 minutes of diazaborine treatment the detected signal shifted towards the nucleoplasm and slightly towards the cytoplasm (Figure 25). Tiny nucleoplasmic accumulation spots were detectable but to a much lesser extent than detected for Nop58 (Figure 24). An enlarged version of the microscopy pictures of Nop4 without and upon 30 minutes of diazaborine treatment is shown in Figure 14.

Isabella Klein and Gertrude Zisser performed TAP-purifications of pre-ribosomal particles at different maturation stages after diazaborine treatment. On the Noc2-particle they found RNA Polymerase I accumulating, suggesting that Noc2 associates with the nascent transcript and the release of the transcript from the polymerase is blocked after diazaborine inhibition. To test this hypothesis, the large subunit of the RNA polymerase I (Rpa190) of the strains expressing Nsa1-GFP and Noc2-GFP was tagged with mCherry. The colocalization of Rpa190 and Nsa1 or Noc2 was investigated by fluorescence microscopy.

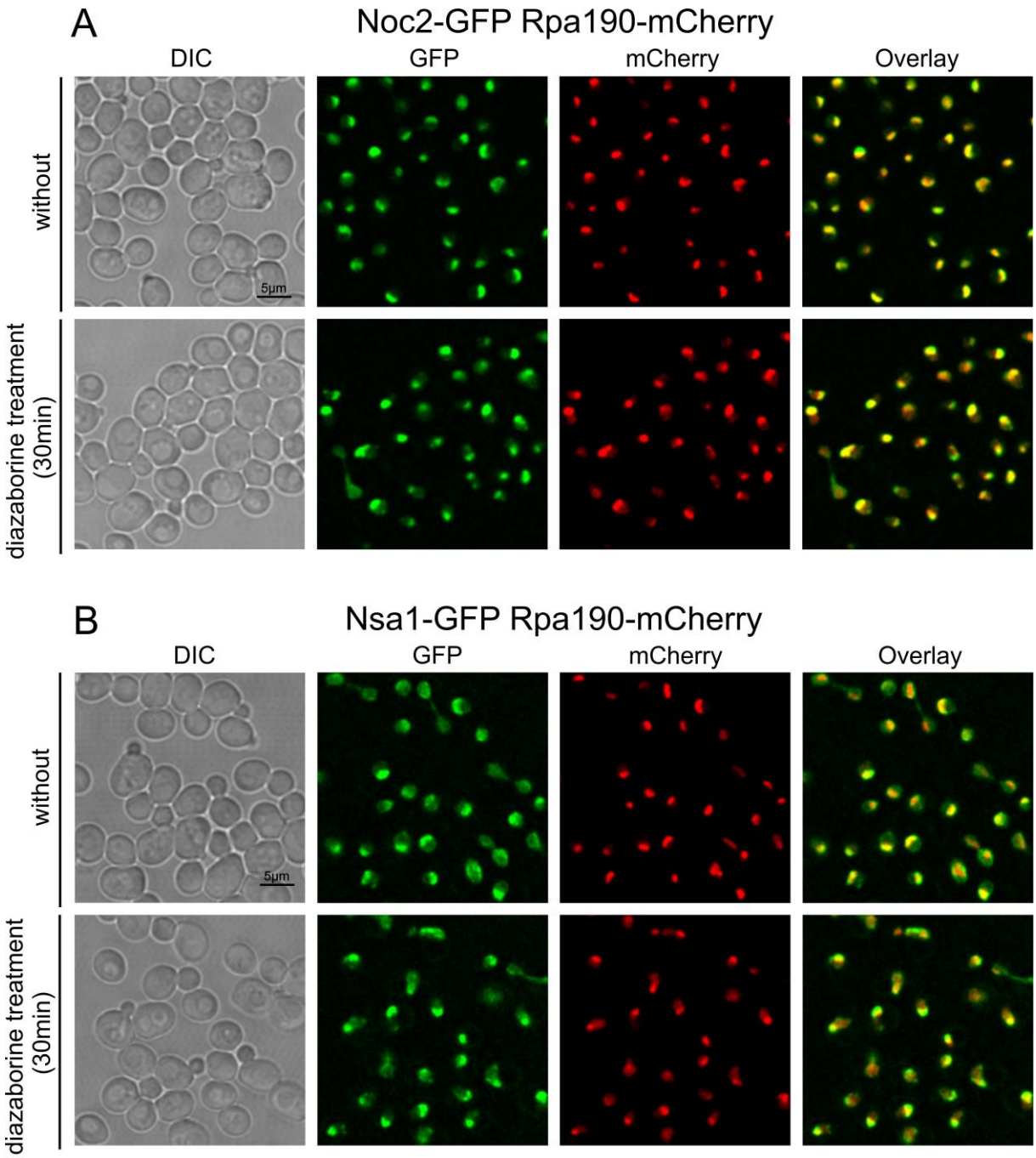

Figure 26: Colocalization studies of Noc2 or Nsa1 with Rpa190 upon diazaborine treatment. Cells were grown and treated according to the standard procedure depicted in 2.11.2.1. The large subunit of RNAPI (Rpa190) showed a strict nucleolar localization without diazaborine treatment. Upon treatment with diazaborine it localized to a bigger extent in the nucleoplasm but did not form any accumulation spots. **(A)** Noc2 showed nucleolar localization and a colocalization with Rpa190 to a very high degree without treatment with diazaborine. After 30 minutes of treatment Noc2 started to form accumulation spots that colocalized with Rpa190 to a lesser extent than before the treatment. **(B)** Nsa1 located in the nucle(ol)us without treatment with diazaborine showing pronounced colocalization with Rpa190. After 30 minutes of treatment Nsa1 formed accumulation spots and colocalized to a lesser extent with Rpa190 than before the treatment.

Without diazaborine treatment Rpa190 showed a high degree of colocalization with Nsa1 as well as with Noc2, assuming a nucleolar localization of Rpa190 without diazaborine treatment. This is consistent with published literature (Albert et al. 2011). After treatment with diazaborine Rpa190 altered its localization by shifting into the nucleoplasm but did not show such spots occurring with Noc2-GFP or Nop58-mCherry. The degree of colocalization was higher with Noc2, than with Nsa1 (Figure 26).

To sum up the above shown results, Noc2 showed a clear nucleolar localization without diazaborine treatment and colocalized to a high degree with Rpa190. Nsa1 showed a nucleolar to nucleoplasmic localization without diazaborine treatment and showed colocalization with Rpa190 to a lesser extent than Noc2. After diazaborine inhibition both maturation factors accumulated in tiny spots but in different areas. In contrast to Nsa1 the accumulating spots of Noc2 colocalized with those of Nop58 and were located in the same region as Rpa190. However, since Rpa190 merely enters the nucleoplasm instead of forming such accumulation spots, it did not seem to be a part of these spots (Figure 27).

3.1.1.4.1 Investigation of Nop58 containing pre-ribosomal particles after diazaborine treatment

To investigate what happens with very early particles and why these accumulation spots occur after diazaborine treatment, the composition of Nop58 containing particles was investigated by performing tandem affinity purification and subsequent western blotting analysis and SDS-PAGE. Therefore cells were treated with diazaborine for 5, 15, 30 and 60 minutes and TAP-purification was performed using magnetic beads. Our group already performed such analysis regarding later particles containing Noc2 and Nsa1. On both particles shuttling factors were depleted after diazaborine treatment (Gertrude Zisser, Isabella Klein, unpublished data). This can be explained be the trapping of shuttling factors in the cytoplasm upon Drg1 inactivation (Loibl et al. 2014).

Upon diazaborine treatment the nucleolar factors Noc1, Noc2, Noc3 and Nop1 did not alter their amount on the Nop58 particles. Merely the nucleolar factor Nop7 seemed to accumulate on the Nop58 particle. The nucleoplasmic factor Noc3 was not detectable on Nop58 containing particles (data not shown). The small subunit of the RNA Polymerase I (Rpa135) also showed an accumulation on the Nop58 particle after approximately 10 minutes of treatment with diazaborine. The same results except the accumulation of Nop7 were obtained by Gertrude Zisser and Isabella Klein by TAP-purifications of Noc2-TAP. The shuttling factors Rlp24 and Nog1 showed contrary behaviour. Whereas Rlp24 diminished after 5 minutes of diazaborine treatment Nog1 rather accumulated slightly. On Noc2 particles both of these shuttling factors diminished upon treatment with diazaborine (Gertrude Zisser, Isabella Klein, unpublished data). Rrp12 initially accumulated on this particle after 10 minutes of diazaborine treatment (Figure 28). However this result is in contrast to Gertrude Zisser,

showing a decrease of Rrp12. The ubiquitin antibody revealed no detectable result (data not shown).

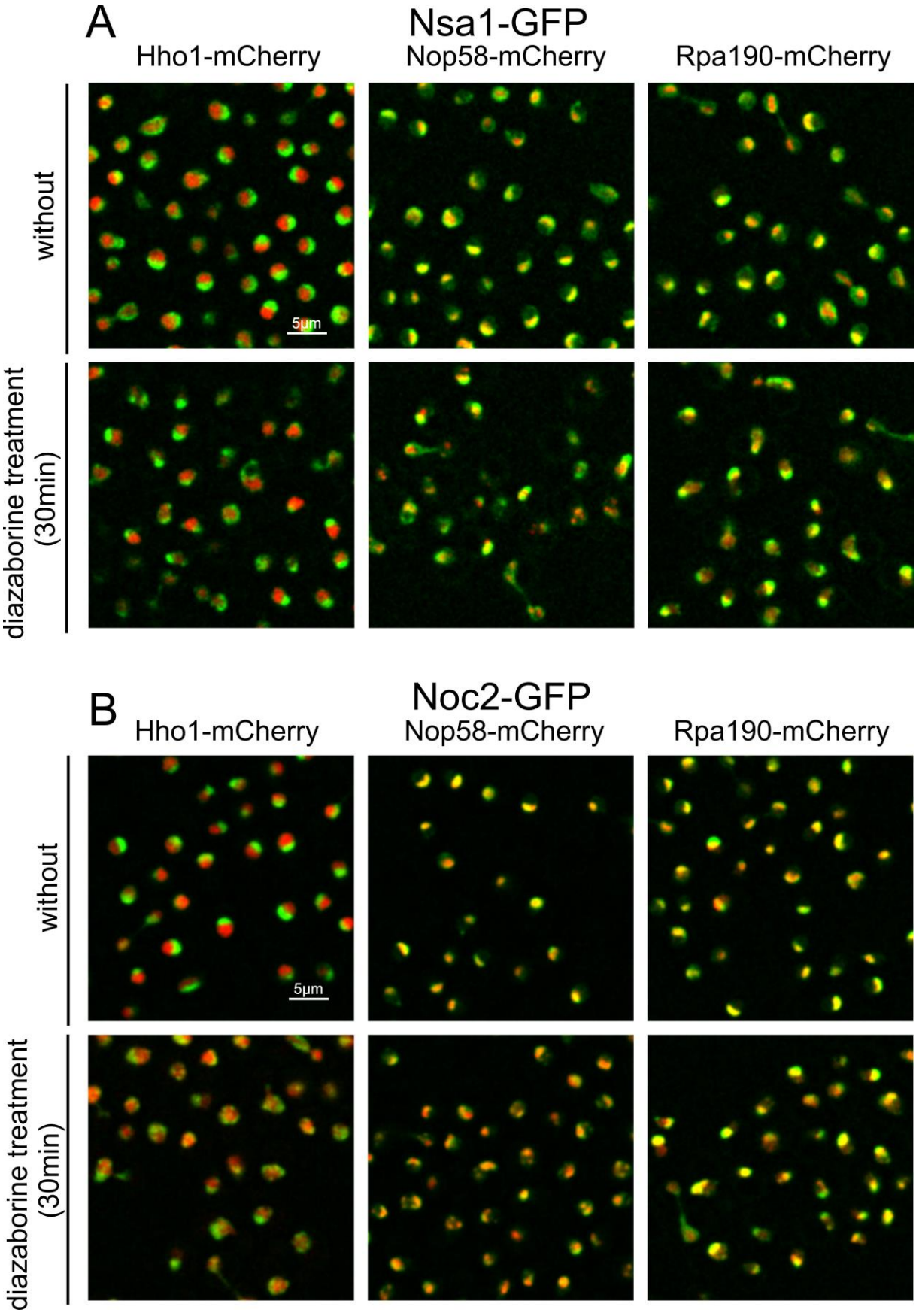

Figure 27: Overview of local alterations of Noc2 and Nsa1 after treatment with diazaborine for 30 minutes. Cells were grown and treated according to the standard procedure depicted in 2.11.2.1. **(A)** Nsa1 located in the nucle(ol)us without diazaborine treatment showing a small degree of colocalization with Hho1 and high degrees with Nop58 and Rpa190. After treatment Nsa1 formed accumulation spots colocating to a high degree with Rpa190 but to a low degree with Hho1 and Nop58. **(B)** Noc2 showed a nucleolar localization without diazaborine treatment, a high colocalization with Nop58 and Rpa190 and no colocalization with Hho1. After 30 minutes of treatment with diazaborine Noc2 formed accumulation spots showing a colocalization with Hho1, Nop58 and Rpa190 to a high extent.

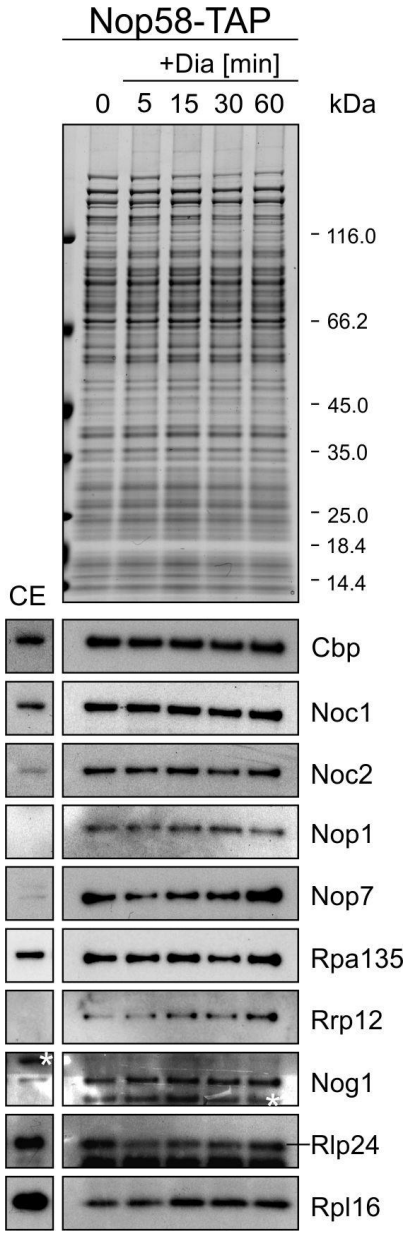

Figure 28: Tandem affinity purification of Nop58-TAP containing particles upon diazaborine treatment. Cells were grown to an OD_{600} of 0.9-1.0 prior to treatment with 100µg/ml diazaborine for indicated periods of time. As a control non treated cell extracts were purified. **(CE)** Crude extracts of non treated cells. The nucleolar factors Noc2, Noc1 and Nop1 did not alter their amount on the particle as well as Nog1. Rlp24 seemed to diminish upon treatment. Rrp12, Rpl16, Rpa135 and Nop7 accumulated on the particle upon treatment. Cross reacting bands with the protein A moiety of the TAP-tag in the crude extract are indicated by a white star.

3.2 Influence of Rpl40 depletion on cytoplasmic particles

The inhibition of Drg1 by diazaborine causes a trapping of shuttling factors in the cytoplasm by the impaired release of Rlp24 (Loibl et al. 2014; Pertschy et al. 2007). The resulting nuclear depletion of this shuttling factors leads to alterations of early particles and disrupt rRNA processing ((Pertschy et al. 2004), Dissertation Isabella Klein). However not only the inactivation of Drg1 can cause an accumulation of shuttling factors in cytoplasm but also the depletion of Rpl40 as previously shown by (Fernández-Pevida et al. 2012). Because the trapping of shuttling factors in the cytoplasm is a prerequisite for all downstream processes, we wanted to investigate how the action of Rpl40 is linked to Drg1.

3.2.1 Investigation of the composition of Arx1 and Bud20 particles after Rpl40 depletion

The investigation of a putative interaction of Rpl40 and Drg1 was done by the investigation of Arx1 and Bud20 particles by tandem affinity purification. The strains harbouring these TAP tagged proteins also included a Rpl40 knockout and carried the *RPL40A* gene on a plasmid additionally to a galactose inducible promotor. Therefore the cells were grown in YPGal, 30°C to an OD_{600} of 0.3-0.4 and transferred to YPD and YPGal as a control and incubated for 4 hours. The cells were lysed and the cell extracts were analysed by TAP-purification and subsequent analysis by western blotting and SDS-PAGE (Figure 29).

Basically all investigated factors diminished in the Arx1 TEV eluate as well as in the Arx1 cell extract except Rsa4, Nmd3 and Drg1. However these results could not be confirmed at a second tandem affinity purification showing the mentioned factors also diminishing after depletion of Rpl40. Since there was no signal obtained for Rei1 and Sqt1 at the first TAP-purification the second TAP purification is also shown for this purpose in Figure 29. Rei1 and Sqt1 diminished after depletion of Rpl40 at least in the crude extract. Rei1 showed the same behavior in the TEV eluate whereas Sqt1 could not be evaluated as a consequence of the weak signal. For the Bud20 particle, all factors showed reduced levels after depletion of Rpl40 in the TEV-eluate and the crude extract except the export factors Sqt1, Mex67 and the cytoplasmic maturation factor Rei1 that seemed to accumulate (Figure 29). However, this could also be caused by differences in the loading amount of the crude extracts. Taken together, these results lead to the assumption of a possible decay of pre-ribosomal particles as a consequence of the depletion of Rpl40. Alternatively both bait proteins could be liberated when Rpl40 is lacking form the particles.

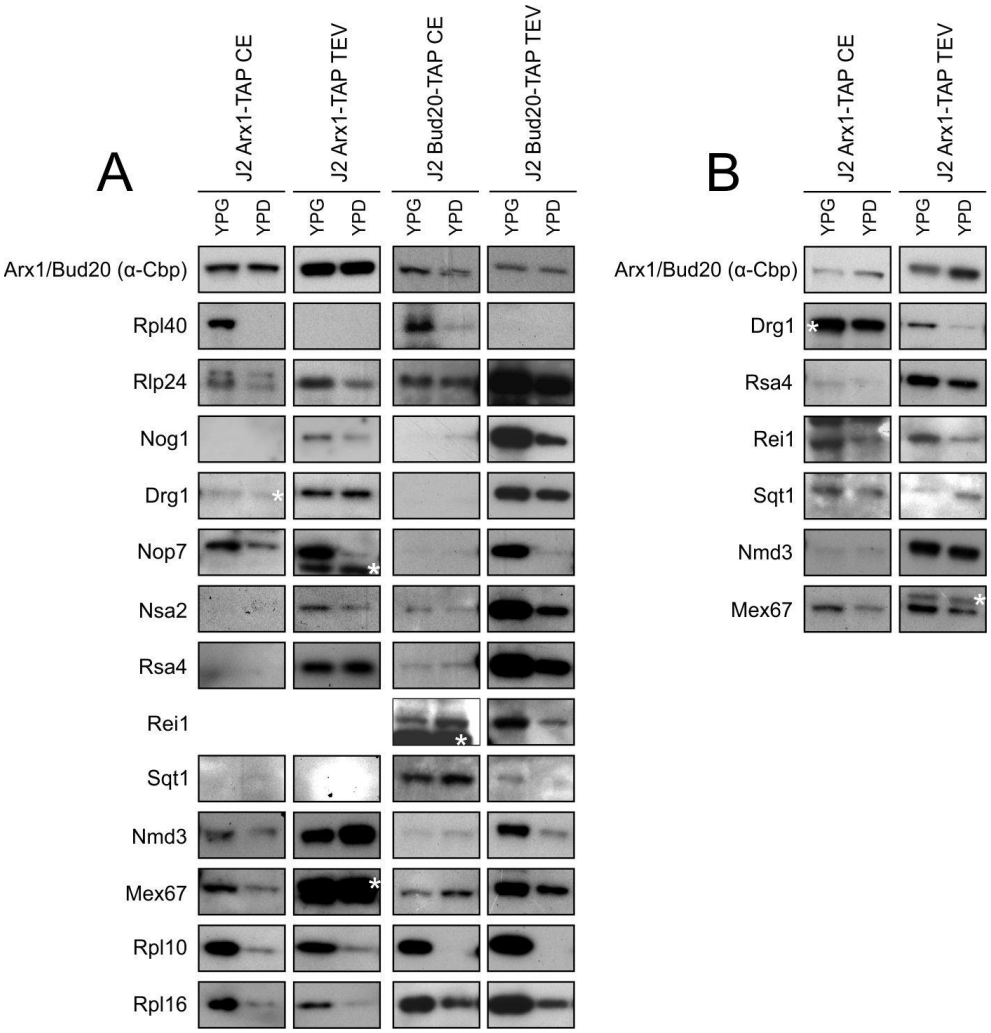

Figure 29: Tandem affinity purification of Arx1 and Bud20 containing particles after depletion of Rpl40. The purification was carried out only until TEV-eluates were obtained. Cells were grown in YPD to an OD_{600} of 0.3-0.4 and shifted to YPG and as a control to YPD for 4 hours. Most factors tested diminished on the investigated particles. The accumulation of Nmd3 and Rsa4 was not confirmed by a second purification. Cross reacting bands with the protein A moiety of the TAP-tag in the crude extract are indicated by a white star.

3.2.2 Investigation of the localization of Arx1 and Bud20 particles after Rpl40 depletion

To test whether the bait proteins show altered localization after depletion of Rpl40, an immunofluorescence of the TAP tagged versions of these proteins was performed. Therefore the cells were grown in YPGal and 30°C to an OD_{600} of 0.3-0.4 and afterwards shifted to YPD for 4 hours. As a control, cells were shifted to YPGal for 4 hours. The TAP-tag was detected by α-Protein A antibodies and visualized by a rhodamine coupled secondary antibody. To distinguish the nucleus, a DAPI staining was performed.

Arx1-TAP showed a steady-state localization in the nucleus and also in the cytoplasm to a small extent while containing an intact Rpl40. Upon depletion of Rpl40 Arx1-TAP seemed to show a cytoplasmic localization to a reduced extent and a slight increased nuclear accumulation. In contrast to these results no alteration of the localization of Bud20-TAP as a consequence of the depletion of Rpl40 was detectable (Figure 30).

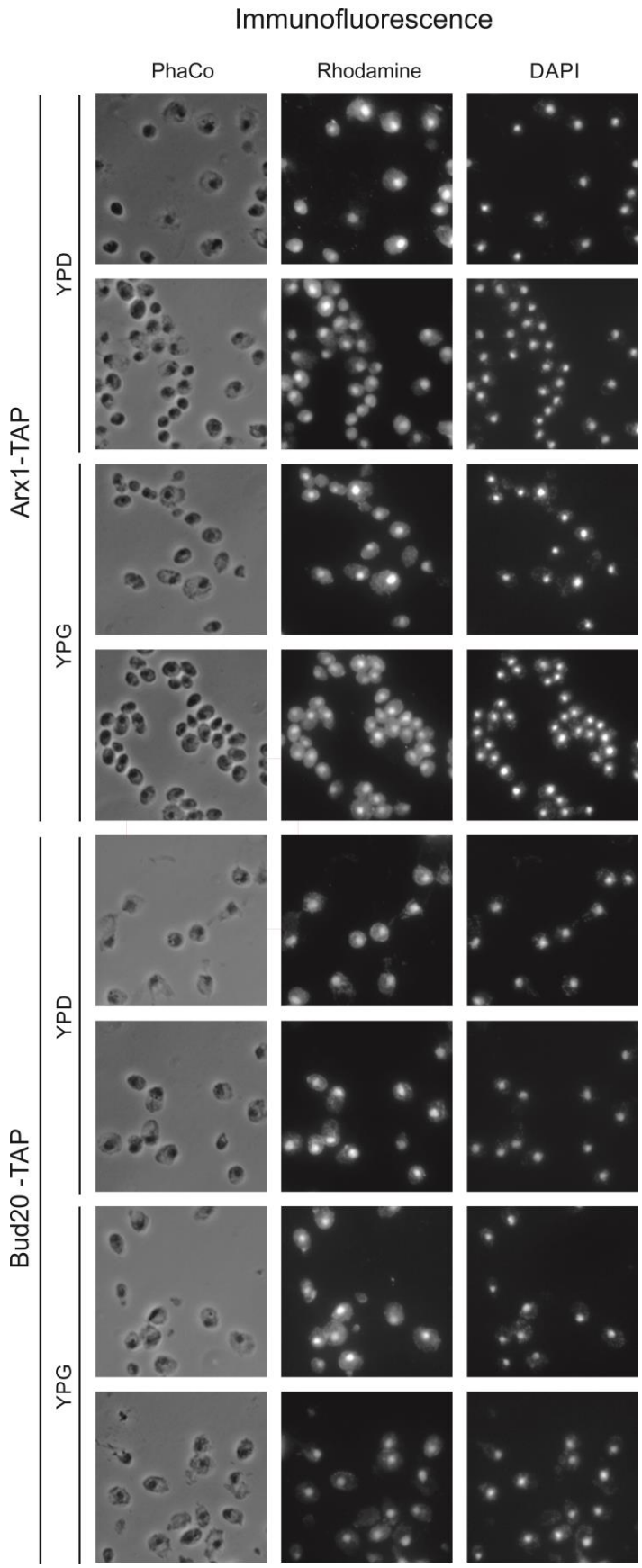

Figure 30: Immunofluorescence of Arx1-TAP and Bud20-TAP after depletion of Rpl40. Cells were grown in YPD to an OD_{600} of 0.3-0.4 and shifted to YPG to deplete Rpl40 for 4 hours. A culture transferred to YPG served as control. TAP-tags were detected using a rabbit α-protein A antibody and secondary rhodamine coupled goat anti-rabbit antibody. Nuclei were detected by DAPI staining. Bud20-TAP did not alter its localization upon Rpl40 depletion. The cytoplasmic signal of Arx1 was reduced after Rpl40 depletion. Two fields for each condition are shown.

4 Discussion

4.1 Effect of diazaborine on the localization of selected pre-60S particles

To elucidate the temporal aspects of the effect of diazaborine on ribosome biogenesis the shuttling factor Nog1, which was already known to accumulate in the cytoplasm upon diazaborine treatment was investigated in detail (Loibl et al. 2014). To mark the nucleoplasm the histone 1 (Hho1) protein was tagged with mCherry. Time series analysis of Nog1-GFP Hho1-mCherry on diazaborine containing agar revealed differences between cells incubated on agar and those propagated in liquid culture, which showed a complete nuclear depletion after 30 minutes of treatment. The remaining nuclear signal of cells treated on diazaborine containing agar suggests that the transfer of the drug from the agar was not efficient enough. In addition to this problem the results of cells treated on diazaborine containing agar could not be reproduced, probably due to the inconstant diazaborine transfer from the agar. Alternatively the hindered oxygen supply on the slide during the incubation period could have slowed down ribosome biogenesis. Thus, the experiments were performed in liquid culture using the test-system Nog1-GFP. For further analysis of the system the known shuttling factors Mrt4 and Tif6 were investigated. Both showed an initial nucleolar to nucleoplasmic localization with tiny spots in these areas. After 30 minutes diazaborine treatment, most of the signal could be detected in the cytoplasm. However, in contrast to Nog1 a significant part of the fluorescence signal could still be detected in the nucleus. These effects were also observed by Claudia Schmidt (2010) and could possibly be explained by the fact that Mrt4 and Tif6 bind earlier to the particles than Nog1 thus requiring a longer time until they are completely transferred to the cytoplasm.

As a control for cytoplasmic accumulation of shuttling proteins after treatment with diazaborine the experiment was also performed by the investigation of the localization of the nucleoplasmic factor Rix1. The analysis revealed a constant nuclear localization over the whole period of treatment.

To monitor the exact cellular localization of the GFP fusions, their localization was related to that of mCherry tagged Hho1. This protein is bound to chromatin and therefore localized in the nucleoplasm. However, the area marked by Hho1 did not seem to fully cover the nucleoplasm. This could be seen by green rings surrounding the additive orange signal of Hho1 (red) and Rix1 (green). Additionally, quantification based on the colocalization with Hho1, yielded solely 70% of Rix1-GFP in the nucleoplasm. Since Rix1 is a strictly nuclear factor, this result seemed to be an underestimation of the actual values. Thus, experiments were continued by marking the whole nucleus with Nic96, which is part of the nuclear envelope. Repeated quantification showed that 90% of Rix1 were located in the nucleus,

likely better reflecting the actual distribution of this protein. Therefore the investigation of Nog1 and Bud20 regarding their shift into the cytoplasm upon diazaborine treatment was performed using Nic96-mCherry as nuclear marker. These experiments showed that Bud20 was transferred completely to the cytoplasm after 10 minutes of diazaborine treatment, whereas it took 30 minutes for Nog1. Basically the quantification seemed to be successful since it revealed a faster transfer of Bud20 into the cytoplasm than of Nog1. This result seemed reasonable since Bud20 is attached to particles at a late nucleoplasmic step contrary to Nog1 being attached at early nucleolar steps (Bassler et al. 2012; Woolford & Baserga 2013). Interestingly after 30 minutes of treatment both shuttling factors showed a remaining signal of approximately 25% in the nucleus. This could reflect systematic errors in data acquisition or data processing, since on the pictures a complete lack of these shuttling factors in the nucleus was observed after 30 minutes of treatment. Alternatively, this phenomenon could be caused solely by optical illusion because sometimes image analysis reveals other results than impressions by eye. Additionally a strong reflexion layer from the laser beam near the cover slide could influence the results, especially since Bud20 and Nog1 are low abundant proteins and exhibit a weak GFP signal. A third possibility to explain the calculated 25% residual signal in the nucleus could be found in *de novo* protein synthesis of Bud20 and Nog1 as a result of the impaired pre-60S maturation. To address this issue, the experiment should be repeated in the presence of cycloheximid to block *de novo* protein synthesis. Since the nucleolar exit of Nog1 seemed to require significant more time than the export into the cytoplasm, the alteration of the nucleolar localization of Nog1 was investigated. For this analysis, mCherry tagged Nop58 served as nucleolar marker. The quantification yielded approximately 21% of Nog1 in the nucleolus without diazaborine treatment. After 10 minutes of treatment solely 7% remained in the nucleolus. The following periods of treatment could not be evaluated due to an occurring fragmentation of the Nop58 mCherry signal.

In addition to the investigation of pre-60S maturation in a temporal manner, nuclear GFP concentrations of Bud20-GFP and Nog1-GFP expressing strains were determined. The results of the GFP quantification revealed a GFP concentration of 11.8±2.2µM in the nucleolus and 7.7±0.9µM in the nucleoplasm of Nog1. The nucleoplasm of Bud20 showed a GFP concentration of 4.0±0.2µM. To evaluate these results, theoretical GFP concentrations were calculated by the use of total number of molecules per cell estimated by Western-blotting of TAP-tagged versions of these proteins (Ghaemmaghami et al. 2003) and the determined cell volume and nucleus/cell ratio (Jorgensen et al. 2002). The calculation based on the literature revealed 15.7µM in the whole nucleus of Nog1 and 3µM in the nucleus of

Bud20. Thus, the GFP quantification of Bud20 and Nog1 estimated in this work is in good agreement to data obtained by a completely different approach.

The fragmentation of the nucleolus upon diazaborine treatment was already described previously using GFP-Nop4 (Pertschy et al. 2004). Since Nop4 is supposed to interact with Nop1, which is attached to Nop58 containing particles, the fragmentation pattern of Nop4 should be very similar to Nop58 (Pertschy et al. 2004; Lafontaine & Tollervey 1999). Anyway this study could not detect the supposed behaviour of Nop4-GFP. This could be caused by the c-terminal GFP tag used for Nop4, since a c-terminal TAP-tag of Nop4 was proposed to cause malfunction of this protein in addition to half-mer formation (Lisa Kappel, unpublished data). Similar spots of ribosomal proteins as observed here were already observed upon inhibition of the export of pre-ribosomal subunits by inactivation of Sda1 and were called “No-body”. Indeed, the so-called “No-bodies” were reported to localize in sub-nucleolar areas marked by the nucleolar marker Nop1 (Dez et al. 2006). Because impaired ribosome biogenesis also affects the nucleolar integrity it is doubtful if Nop1 is a suitable marker for the investigation of the nucleolar localization. Thus, the localization of Nop58 being part of the same particle as Nop1 (Lafontaine & Tollervey 1999) was investigated by the nucleoplasmic marker Rix1 which did not change its localization upon diazaborine treatment (Kressler et al. 2008). Treatment with diazaborine revealed spots of Nop58-mCherry colocalized with Rix1-GFP and hence indicating a nucleoplasmic localization. This results disagree with the afore mentioned publication by Dez et al. 2006.

For further investigation of the impact of diazaborine on early steps of ribosome biogenesis the localization of the nucle(ol)ar factors Noc2 and Nsa1 was examined. Noc2 showed a high degree of colocalization with Nop58 without as well as with diazaborine treatment. Also the investigation concerning the nucleoplasmic localization of Noc2 revealed a shift into the nucleoplasm upon diazaborine treatment as was observed for Nop58. The late nucleolar to nucleoplasmic factor Nsa1 (Kressler et al. 2010) showed colocalization with Nop58 to a lesser extent. Although spots were detected for Nsa1, they did not seem to colocalize with spots formed from Nop58. The colocalization study with Hho1 revealed a reduced localization in the nucleoplasm for Nsa1 compared to Noc2. Because Gertrude Zisser and Isabella Klein (unpublished data) described an accumulation of the small and the large subunit of RNA polymerase I (Rpa135, Rpa190) on nucleolar particles upon diazaborine treatment, the large subunit of RNA polymerase I was tagged with mCherry prior to localization studies. We found that the RNA polymerase I seemed to enter the nucleoplasm upon diazaborine treatment in contrast to the initial nucleolar localization. This could be a hint for nucleolar chromatin decondensation and its extension into the nucleoplasm upon

inhibition of ribosome biogenesis. However, Rpa190 was not enriched in the occurring spots neither formed by Noc2 nor by Nsa1. These results somehow contradict with the findings of Isabella Klein and Gertrude Zisser. This finding could be explained by the fact, that only limited amounts of RNA polymerase I co-purified with the Nsa1 particle but the bulk was transferred into the nucleoplasm and detected by fluorescence microscopy.

To gain further information about the sites of accumulation, TAP-purifications of Nop58 in the absence and presence of diazaborine were performed. The SDS-PAGE of the obtained TAP-purification yielded several alterations of band intensities over the period of treatment with high molecular weight assuming UTPs (Pérez-Fernández et al. 2007). These bands have to be further investigated by mass spectrometry. In addition to SDS-PAGE the TAP-purification was also examined by western blotting. Basically there were not many alterations in the composition of the Nop58-TAP particle detectable after diazaborine treatment in contrast to Noc2-TAP and Nsa1-TAP, which were analysed by Gertrude Zisser and Isabella Klein (unpublished data). The nucleolar factors Noc1 and Noc2 as well as Nop1 did not alter their amount on the Nop58 particle. Since Nop1 assembles together with Nop58 to the pre-35S rRNA forming the SSU processome, this result was not unexpected (Tschochner & Hurt 2003). Noc1 and Noc2 are also thought to assemble co-transcriptionally forming together with other factors and the SSU processome the 90S particle (Hierlmeier et al. 2013). These results confirmed our colocalization studies revealing a colocalization between Noc2 and Nop58 to a very high extent even upon diazaborine treatment. The nucleolar to nucleoplasmic factor Nop7 showed a slight accumulation over the period of treatment also indicating a reduced release from the Nop58-TAP particle. This result was also obvious by fluorescence microscopy, showing a more pronounced nucleolar localization after diazaborine treatment (Pertschy et al. 2004). An accumulation of the small subunit of RNA polymerase I was observed at Nop58 containing particles as for TAP purifications of Noc2 containing particles. However, a novel TAP-purification of Nop58-TAP showing similar amounts of Rpa135 over the whole period of treatment could not verify the result of this study (Gertrude Zisser, unpublished data). The result obtained by Gertrude Zisser would be in line with the results obtained from fluorescence microscopy of this study. Contradicting results were also observed regarding the amount of Rrp12 on Nop58 particles. In this work Rrp12 seemed to accumulate upon treatment with diazaborine, whereas Gertrude Zisser showed that it diminished. In this case, the experiments have to be repeated to elucidate the behaviour of Rrp12 upon diazaborine inhibition. In contrast to Noc2 or Nsa1 particles the shuttling factor Nog1 was present in low amounts of the Nop58-particle and did not diminish upon treatment. However, the shuttling factor Rlp24 showed a slight decrease upon treatment. For Rlp24 similar results were obtained by Gertrude Zisser. Since Rlp24 binds

earlier to pre-60S particles than Nog1 (Saveanu et al. 2003) and diminishes upon diazaborine treatment, Nog1 might not be present in Nop58-particles actually. Thus, indicating a contamination of the Nop58 particle with Nog1 or a cross-reaction with the Nog1 antibody. The investigation regarding a possible ubiquitination, hence indicating protein decay after diazaborine treatment yielded no detectable results. Assuming the localization of Nop58 in “No-bodies” upon diazaborine treatment this result would indicate decoupled protein degradation from RNA degradation in case of impaired pre-60S maturation. This result was strengthened by the finding that the proteasome did not colocalize with “No-bodies” upon impaired ribosome biogenesis (Dez et al. 2006).

To sum up the investigation regarding the temporal aspects of the localization of Nog1 and Bud20 upon diazaborine treatment seemed to be successful and can serve as starting point for further, more detailed examinations. The result that about 25% of the Nog1 and Bud20 particles are remaining in the nucleus after 30 minutes of treatment has to be further investigated. This could be done by inhibiting *de novo* protein synthesis by cycloheximid. The quantification of Nog1-GFP and Bud20-GFP using various GFP concentrations added *in vitro* to the afore mentioned strains also seemed to be successful and well worth to extend to other pre-ribosomal maturation factors. The investigation of the impact of diazaborine on early particles revealed an accumulation of early particles in subnucleoplasmic sides. However, if this accumulation sites indeed correspond to degradation of aberrant pre-ribosomes remains to be elucidated. The early nucleolar Noc2 and the late nucleolar to nucleoplasmic Nsa1 exhibited different sites of accumulation upon diazaborine inhibition. Thus, indicating different surveillance systems for particles at different maturation stages. This assumption is also described in literature (Lafontaine 2010).

4.2 Impact of Rpl40 depletion on cytoplasmic pre-60s maturation

A recent publication showed an impaired release of Rlp24 and Nmd3 caused by a depletion of the cytoplasmic ribosomal protein Rpl40 (Fernández-Pevida et al. 2012). Since the inactivation of Drg1 causes a similar phenotype (Kappel et al. 2012), a putative connection between Drg1 and Rpl40 was investigated. Therefore strains harbouring a double knockout of the native *RPL40A* and *RPL40B* genes and carrying a plasmid containing a HA-tagged version of *RPL40A* under a galactose inducible promoter were used. The investigated strains were grown in YPG prior to shift to YPD for 4 hours for depletion of Rpl40. Under these conditions Bud20 and Arx1 containing particles were investigated by TAP-purification and western blotting. The analysis of Arx1 containing particles revealed a decrease of all investigated proteins including the ribosomal proteins Rpl10 and Rpl16. The factors Drg1, Rsa4, Nmd3 and Mex67 could not be evaluated since they showed contrary behaviour in a second TAP-purification. In contrast to Arx1, the Bud20 containing particles exhibited a reproducible decrease of all investigated factors. A similar experiment was already

performed by Anna Gungl whereas the depletion of Rpl40 was carried out solely for 2h revealing no significant alterations of the particles composition except a decrease of the ribosomal proteins Rpl25 and Rpl16. Since the effect of the depletion of Rpl40 was shown not until 9h (Fernández-Pevida et al. 2012), 2h of depletion might have been too short to gain a significant effect. Nevertheless a beginning detachment of ribosomal proteins was observed. The decrease of ribosomal proteins was also observed in this study in addition to a decrease of all maturation factors investigated.

This result leads to the assumption of a decay of the observed ribosomal particles. To test whether the localization of the bait proteins changes upon Rpl40 depletion, further investigations were carried out by immunofluorescence. Thereby Arx1 showed a slight decrease in cytoplasmic localization after depletion of Rpl40 whereas Bud20 did not show any alterations at all. Fernández-Pevida et al. could show a regular release of all maturation factors except Rlp24 and Nmd3 after the Rpl40 depletion (Fernández-Pevida et al. 2012). Since Bud20 and Arx1 showed a more or less nucleoplasmic localization after Rpl40 depletion, these factors can be released in the cytoplasm and recycled back into the nucleus. Indeed, the depletion of Rpl40 seemed to prevent binding of recycled Arx1 and Bud20 to nuclear particles since other particle components were co-purified in reduced amounts after Rpl40 depletion. This hypothesis is strengthened by the observation of Fernández-Pevida et al., that the depletion of Rpl40 causes a nuclear export defect seen by accumulated ribosomal proteins in the nucleus (Fernández-Pevida et al. 2012). This assumption leads to the speculation that in our study mainly unbound shuttling factors were purified after Rpl40 depletion. For further investigation of the effect of the depletion of Rpl40 the composition of Rpl24 containing particles should be examined, since Rlp24 stays attached to particles even upon Rpl40 depletion (Fernández-Pevida et al. 2012). Such an experiment could help to clarify the relationship of Drg1 and Rpl40.

References

Albert, B. et al., 2011. RNA polymerase I-specific subunits promote polymerase clustering to enhance the rRNA gene transcription cycle. *Journal of Cell Biology*, 192(2), pp.277–293.

Bassler, J. et al., 2012. The conserved Bud20 zinc finger protein is a new component of the ribosomal 60S subunit export machinery. *Molecular and Cellular Biology*, 32(24), pp.4898–4912.

Bergler, H. et al., 1994. Protein EnvM is the NADH-dependent enoyl-ACP reductase (FabI) of Escherichia coli. *Journal of Biological Chemistry*, 269(7), pp.5493–5496.

Bernstein, K. a. et al., 2004. The small-subunit processome is a ribosome assembly intermediate. *Eukaryotic Cell*, 3(6), pp.1619–1626.

Block, M.R. et al., 1988. Purification of an N-ethylmaleimide-sensitive protein catalyzing vesicular transport. *Proceedings of the National Academy of Sciences of the United States of America*, 85(November), pp.7852–7856.

Bradatsch, B. et al., 2007. Arx1 Functions as an Unorthodox Nuclear Export Receptor for the 60S Preribosomal Subunit. *Molecular Cell*, 27, pp.767–779.

Demoinet, E. et al., 2007. The Hsp40 chaperone Jjj1 is required for the nucleo-cytoplasmic recycling of preribosomal factors in Saccharomyces cerevisiae. *RNA (New York, N.Y.)*, 13, pp.1570–1581.

Dez, C., Houseley, J. & Tollervey, D., 2006. Surveillance of nuclear-restricted pre-ribosomes within a subnucleolar region of Saccharomyces cerevisiae. *The EMBO journal*, 25(7), pp.1534–1546.

Dez, C. & Tollervey, D., 2004. Ribosome synthesis meets the cell cycle. *Current Opinion in Microbiology*, 7, pp.631–637.

Dragon, F. et al., 2002. A large nucleolar U3 ribonucleoprotein required for 18S ribosomal RNA biogenesis. *Nature*, 417(June), pp.967–970.

Fernández-Pevida, A. et al., 2012. Yeast ribosomal protein L40 assembles late into precursor 60 S ribosomes and is required for their cytoplasmic maturation. *Journal of Biological Chemistry*, 287, pp.38390–38407.

French, S.L. et al., 2003. In exponentially growing Saccharomyces cerevisiae cells, rRNA synthesis is determined by the summed RNA polymerase I loading rate rather than by the number of active genes. *Molecular and cellular biology*, 23(5), pp.1558–1568.

Fromont-Racine, M. et al., 2003. Ribosome assembly in eukaryotes. *Gene*, 313, pp.17–42.

Gallagher, J.E.G. et al., 2004. RNA polymerase I transcription and pre-rRNA processing are linked by specific SSU processome components. *Genes and Development*, 18, pp.2507–2517.

Ghaemmaghami, S. et al., 2003. Global analysis of protein expression in yeast. *Nature*, 425(1997), pp.737–741. Available at:

http://www.ncbi.nlm.nih.gov/entrez/query.fcgi?cmd=Retrieve&db=PubMed&dopt=Citation&list_uids=14562106.

Gietz, R.D. et al., 1995. Studies on the transformation of intact yeast cells by the LiAc/SS-DNA/PEG procedure. *Yeast*, 11, pp.355–360.

Grassberger, M. a, Turnowsky, F. & Hildebrandt, J., 1984. Preparation and antibacterial activities of new 1,2,3-diazaborine derivatives and analogues. *Journal of medicinal chemistry*, 27(4), pp.947–953.

Hedges, J., West, M. & Johnson, A.W., 2005. Release of the export adapter, Nmd3p, from the 60S ribosomal subunit requires Rpl10p and the cytoplasmic GTPase Lsg1p. *The EMBO journal*, 24(3), pp.567–579.

Henras, a. K. et al., 2008. The post-transcriptional steps of eukaryotic ribosome biogenesis. *Cellular and Molecular Life Sciences*, 65, pp.2334–2359.

Hierlmeier, T. et al., 2013. Rrp5p, Noc1p and Noc2p form a protein module which is part of early large ribosomal subunit precursors in S. cerevisiae. *Nucleic Acids Research*, 41(2), pp.1191–1210.

Ho, J.H., Kallstrom, G. & Johnson, a W., 2000. Nmd3p is a Crm1p-dependent adapter protein for nuclear export of the large ribosomal subunit. *The Journal of cell biology*, 151(5), pp.1057–1066.

Van Hoof, a, Lennertz, P. & Parker, R., 2000. Three conserved members of the RNase D family have unique and overlapping functions in the processing of 5S, 5.8S, U4, U5, RNase MRP and RNase P RNAs in yeast. *The EMBO journal*, 19(6), pp.1357–1365.

Hoskins, J.R. et al., 1998. The role of the ClpA chaperone in proteolysis by ClpAP. *Proceedings of the National Academy of Sciences of the United States of America*, 95(October), pp.12135–12140.

Hurt, E. et al., 1999. A novel in vivo assay reveals inhibition of ribosomal nuclear export in Ran-cycle and nucleoporin mutants. *Journal of Cell Biology*, 144(3), pp.389–401.

Jorgensen, P. et al., 2002. Systematic identification of pathways that couple cell growth and division in yeast. *Science (New York, N.Y.)*, 297(September), pp.395–400.

Kappel, L. et al., 2012. Rlp24 activates the AAA-ATPase Drg1 to initiate cytoplasmic pre-60S maturation. *Journal of Cell Biology*, 199(5), pp.771–782.

Kemmler, S. et al., 2009. Yvh1 is required for a late maturation step in the 60S biogenesis pathway. *Journal of Cell Biology*, 186(6), pp.863–880.

Koš, M. & Tollervey, D., 2010. Yeast Pre-rRNA Processing and Modification Occur Cotranscriptionally. *Molecular Cell*, 37(6), pp.809–820. Available at: http://dx.doi.org/10.1016/j.molcel.2010.02.024.

Kressler, D. et al., 2008. The AAA ATPase Rix7 powers progression of ribosome biogenesis by stripping Nsa1 from pre-60S particles. *Journal of Cell Biology*, 181(type I), pp.935–944.

Kressler, D. et al., 2012. The power of AAA-ATPases on the road of pre-60S ribosome maturation - Molecular machines that strip pre-ribosomal particles. *Biochimica et Biophysica Acta - Molecular Cell Research*, 1823(1), pp.92–100. Available at: http://dx.doi.org/10.1016/j.bbamcr.2011.06.017.

Kressler, D., Hurt, E. & Baßler, J., 2010. Driving ribosome assembly. *Biochimica et Biophysica Acta - Molecular Cell Research*, 1803, pp.673–683.

Lafontaine, D.L. & Tollervey, D., 1999. Nop58p is a common component of the box C+D snoRNPs that is required for snoRNA stability. *RNA (New York, N.Y.)*, 5, pp.455–467.

Lafontaine, D.L.J., 2010. A “garbage can” for ribosomes: how eukaryotes degrade their ribosomes. *Trends in Biochemical Sciences*, 35(5), pp.267–277. Available at: http://dx.doi.org/10.1016/j.tibs.2009.12.006.

Lebreton, A. et al., 2006. A functional network involved in the recycling of nucleocytoplasmic pre-60S factors. *Journal of Cell Biology*, 173(3), pp.349–360.

Leporé, N. & Lafontaine, D.L.J., 2011. A functional interface at the rDNA connects rRNA synthesis, pre-rRNA processing and nucleolar surveillance in budding yeast. *PLoS ONE*, 6(9).

Lo, K.Y. et al., 2010. Defining the pathway of cytoplasmic maturation of the 60S ribosomal subunit. *Molecular Cell*, 39(2), pp.196–208.

Lo, K.Y. et al., 2009. Ribosome stalk assembly requires the dual-specificity phosphatase Yvh1 for the exchange of Mrt4 with P0. *Journal of Cell Biology*, 186(6), pp.849–862.

Loibl, M. et al., 2014. The drug diazaborine blocks ribosome biogenesis by inhibiting the AAA-ATPase drg1. *Journal of Biological Chemistry*, 289, pp.3913–3922.

Menne, T.F. et al., 2007. The Shwachman-Bodian-Diamond syndrome protein mediates translational activation of ribosomes in yeast. *Nature genetics*, 39(4), pp.486–495.

Meyer, A.E. et al., 2007. The specialized cytosolic J-protein, Jjj1, functions in 60S ribosomal subunit biogenesis. *Proceedings of the National Academy of Sciences of the United States of America*, 104(5), pp.1558–1563.

Moy, T.I. & Silver, P. a., 1999. Nuclear export of the small ribosomal subunit requires the Ran-GTPase cycle and certain nucleoporins. *Genes and Development*, 13, pp.2118–2133.

Panse, V.G. & Johnson, A.W., 2010. Maturation of eukaryotic ribosomes: acquisition of functionality. *Trends in Biochemical Sciences*, 35(5), pp.260–266.

Pérez-Fernández, J. et al., 2007. The 90S preribosome is a multimodular structure that is assembled through a hierarchical mechanism. *Molecular and cellular biology*, 27(15), pp.5414–5429.

Pertschy, B. et al., 2007. Cytoplasmic recycling of 60S preribosomal factors depends on the AAA protein Drg1. *Molecular and cellular biology*, 27(19), pp.6581–6592.

Pertschy, B. et al., 2004. Diazaborine treatment of yeast cells inhibits maturation of the 60S ribosomal subunit. *Molecular and cellular biology*, 24(14), pp.6476–6487.

Pertschy, B. et al., 2009. RNA helicase Prp43 and its co-factor Pfa1 promote 20 to 18 S rRNA processing catalyzed by the endonuclease Nob1. *Journal of Biological Chemistry*, 284(50), pp.35079–35091.

Rodríguez-Mateos, M. et al., 2009. The amino terminal domain from Mrt4 protein can functionally replace the RNA binding domain of the ribosomal P0 protein. *Nucleic Acids Research*, 37(11), pp.3514–3521.

Rudra, D. & Warner, J.R., 2004. What better measure than ribosome synthesis? *Genes and Development*, 18(718), pp.2431–2436.

Saveanu, C. et al., 2003. Sequential protein association with nascent 60S ribosomal particles. *Molecular and cellular biology*, 23(13), pp.4449–4460.

Schindelin, J. et al., 2012. Fiji: an open source platform for biological image analysis. *Nature Methods*, 9(7), pp.676–682.

Schuch, B. et al., 2014. form a composite surface for recruiting the. , 33(23), pp.2829–2847.

Seiser, R.M. et al., 2006. Ltv1 is required for efficient nuclear export of the ribosomal small subunit in Saccharomyces cerevisiae. *Genetics*, 174(October), pp.679–691.

Senger, B. et al., 2001. The nucle(ol)ar Tif6p and Efl1p are required for a late cytoplasmic step of ribosome synthesis. *Molecular Cell*, 8, pp.1363–1373.

Strunk, B.S. et al., 2012. Initiation by 40S Assembly Intermediates. , 333(6048), pp.1449–1453.

Thiry, M. & Lafontaine, D.L.J., 2005. Birth of a nucleolus: The evolution of nucleolar compartments. *Trends in Cell Biology*, 15(4), pp.194–199.

Thorsness, P.E., White, K.H. & Ong, W.C., 1993. AFG2, an essential gene in yeast, encodes a new member of the Sec18p, Pas1p, Cdc48p, TBP-1 family of putative ATPases. *Yeast*, 9, pp.1267–1271.

Tschochner, H. & Hurt, E., 2003. Pre-ribosomes on the road from the nucleolus to the cytoplasm. *Trends in Cell Biology*, 13(5), pp.255–263.

Udem, S. a & Warner, J.R., 1972. Ribosomal RNA synthesis in Saccharomyces cerevisiae. *Journal of molecular biology*, 65, pp.227–242.

Venema, J. & Tollervey, D., 1999. Ribosome synthesis in Saccharomyces cerevisiae. *Annual review of genetics*, 33, pp.261–311.

Warner, J.R., 1999. The economics of ribosome biosynthesis in yeast. *Trends in Biochemical Sciences*, 24(November), pp.437–440.

West, M. et al., 2005. Defining the order in which Nmd3p and Rpl10p load onto nascent 60S ribosomal subunits. *Molecular and cellular biology*, 25(9), pp.3802–3813.

White, S.R. & Lauring, B., 2007. AAA+ ATPases: Achieving diversity of function with conserved machinery. *Traffic*, 8, pp.1657–1667.

Woolford, J.L. & Baserga, S.J., 2013. Ribosome biogenesis in the yeast Saccharomyces cerevisiae. *Genetics*, 195(November), pp.643–681.

Yao, W. et al., 2007. Nuclear Export of Ribosomal 60S Subunits by the General mRNA Export Receptor Mex67-Mtr2. *Molecular Cell*, 26, pp.51–62.

Yao, Y. et al., 2010. Ecm1 is a new pre-ribosomal factor involved in pre-60S particle export. *RNA (New York, N.Y.)*, 16, pp.1007–1017.

Ye, Y., Meyer, H.H. & Rapoport, T. a, 2001. The AAA ATPase Cdc48/p97 and its partners transport proteins from the ER into the cytosol. *Nature*, 414(December), pp.652–656.

Zakalskiy, A. et al., 2002. Structural and enzymatic properties of the AAA protein Drglp from Saccharomyces cerevisiae. Decoupling of intracellular function from ATPase activity and hexamerization. *Journal of Biological Chemistry*, 277(30), pp.26788–26795.

Claudia Schmidt, 2010. Investigation of late cytoplasmic pre-60S maturation steps. Masterarbeit an der Karl-Franszens-Universität Graz

5 Supplemental material

Raw data derived by GFP quantification and calculated kinetics of Bud20-GFP, Nog1-GFP and Rix1-GFP

Bud20-GFP Nic96-mCherry

diazaborine treatment [min]	0	2	5	10	15	30
Nucleus (raw intensity)	16633690	6037154	3675792	4641793	3729155	4048855
	13696266	6656781	8537239	6769786	5650321	6760094
	13714426	2357199	3607230	5781680	6346800	7036122
Cytoplasm (raw intensity)	2088385	11171981	12596305	21282328	20030761	16083657
	904008	11973959	16794854	19504482	18503844	17984469
	1791143	3287262	7761662	19357320	19957315	22664208
Total (raw intensity)	18722075	17209135	16272097	25924121	23759916	20132512
	14600274	18630740	25332093	26274268	24154165	24744563
	15505569	5644461	11368892	25139000	26304115	29700330
%Signal nucleus	88,845334	35,081101	22,589541	17,905305	15,695152	20,111027
	93,808281	35,730094	33,701278	25,765841	23,39274	27,319513
	88,448389	41,761277	31,728949	22,998846	24,128544	23,690383
Mean	**90,367334**	**37,524157**	**29,339923**	**22,223331**	**21,072145**	**23,706974**
Standard deviation	2,9865488	3,6837733	5,9285968	3,9872387	4,6711234	3,6042712

Nog1-GFP Nic96-mCherry

diazaborine treatment [min]	0	2	5	10	15	30
Nucleus (raw intensity)	14044341	24455650	4009871	12754918	14706825	6329382
	15422418	11808437	7603243	3681582	4979340	2992726
	11352840	5545291	4283573	4562112	4549578	4837272
Cytoplasm (raw intensity)	4634282	5936826	2228268	16092746	17959680	18604447
	2606736	4341287	5984168	4110511	6809719	6971367
	1947359	1714142	2866593	4580350	5663789	10032980
Total (raw intensity)	18678623	30392476	6238139	28847664	32666505	24933829
	18029154	16149724	13587411	7792093	11789059	9964093
	13300199	7259433	7150166	9142462	10213367	14870252
%Signal nucleus	75,189381	80,466132	64,279924	44,214734	45,021116	25,384717
	85,541551	73,118507	55,957997	47,247665	42,236959	30,035107
	85,358422	76,387385	59,908721	49,900257	44,54533	32,529859
Mean	**82,029785**	**76,657341**	**60,048881**	**47,120885**	**43,934468**	**29,316561**
Standard deviation	5,9246711	3,6812442	4,1627336	2,8448806	1,4892099	3,6263609

Nog1-GFP Nop58-mCherry

diazaborine treatment [min]	0	2	5	10
Nucleus (raw intensity)	4556701	1178443	1609701	825580
	3093595	1636437	2029440	394999
	4230240	1281934	640349	1214453
Cytoplasm (raw intensity)	14881207	6892268	18157546	12787882
	12224598	9281062	20248440	6110476
	16570910	5169265	9494655	14858638
Total (raw intensity)	19437908	8070711	19767247	13613462
	15318193	10917499	22277880	6505475
	20801150	6451199	10135004	16073091
%Signal nucleus	23,442343	14,601477	8,1432736	6,0644383
	20,195561	14,98912	9,1096639	6,0717934
	20,336568	19,871252	6,3181919	7,5558149
Mean	**21,324824**	**16,487283**	**7,8570431**	**6,5640155**
Standard deviation	1,8351799	2,9370055	1,4175771	0,8589313

Rix1-GFP Nic96-mCherry

diazaborine treatment [min]	0	2	5	10	15	30
Nucleus (raw intensity)	6034165	9108066	15308909	9543031	4729850	14420487
	8005532	8258307	7027283	6713578	7594746	6017707
	9581187	7103301	8625877	7298235	8962360	8592828
Cytoplasm (raw intensity)	431696	1132826	1743678	1075414	527610	611016
	413803	651178	239213	445960	422552	849556
	1774031	408657	570107	284211	700982	736550
Total (raw intensity)	6465861	10240892	17052587	10618445	5257460	15031503
	8419335	8909485	7266496	7159538	8017298	6867263
	11355218	7511958	9195984	7582446	9663342	9329378
%Signal nucleus	93,323457	88,93821	89,774701	89,872208	89,964546	95,935097
	95,085087	92,691183	96,708001	93,771107	94,729496	87,6289
	84,376953	94,559914	93,800479	96,251724	92,745967	92,105047
Mean	**90,928499**	**92,063102**	**93,427727**	**93,298346**	**92,480003**	**91,889681**
Standard deviation	5,7417678	2,8629972	3,4816474	3,2159263	2,3935833	4,1572847